

Energetically Trapped Triplet Excitons and their Generation Pathways in Organic Solar Cell Blends based on (Non-) Halogenated PBDB-T and Y-Series

Jeannine Grüne^{1*}, Giacomo Londi², Alexander J. Gillett³, Basil Stähly¹, Sebastian Lulei¹, Maria Kotova¹, Yoann Olivier², Vladimir Dyakonov¹, and Andreas Sperlich^{1*}

¹Experimental Physics 6, Julius Maximilian University of Würzburg, Am Hubland, 97074 Würzburg, Germany

²Laboratory for Computational Modeling of Functional Materials, Namur Institute of Structured Matter, University of Namur, Rue de Bruxelles, 61, 5000 Namur, Belgium

³Cavendish Laboratory, University of Cambridge, JJ Thomson Avenue, Cambridge, UK

* jeannine.gruene@physik.uni-wuerzburg.de, sperlich@physik.uni-wuerzburg.de

Abstract

The great progress in organic photovoltaics (OPV) over the past few years has been largely achieved by the development of non-fullerene acceptors (NFAs), with power conversion efficiencies now approaching 20%. To further improve device performance, loss mechanisms must be identified and minimized. Triplet states are known to adversely affect device performance, since they can form energetically trapped excitons on low-lying states that are responsible for non-radiative losses or even device degradation. Halogenation of OPV materials has long been employed to tailor energy levels and to enhance open circuit voltage. Yet, the influence on recombination to triplet excitons has been largely unexplored. Using the complementary spin-sensitive methods of photoluminescence detected magnetic resonance (PLDMR) and transient electron paramagnetic resonance (trEPR) corroborated by transient absorption and quantum-chemical calculations, we unravel exciton pathways in OPV blends employing the polymer donors PBDB-T, PM6 and PM7 together with NFAs Y6 and Y7. All blends reveal triplet excitons on the NFA populated via non-geminate hole back transfer and, in blends with halogenated donors, also by spin-orbit coupling driven intersystem crossing. Identifying these triplet formation pathways in all tested solar cell absorber films highlights the untapped potential for improved charge generation to further increase plateauing OPV efficiencies.

Keywords: Organic Photovoltaics; Triplet Excitons; Non-Fullerene Acceptors; Halogenation; Spin Resonance

Introduction

Organic solar cells (OSC) based on non-fullerene acceptors (NFAs) have attracted much attention due to their strong absorption in the visible and near infrared spectral regions and their energy-level tunability, in contrast to fullerene acceptors.^[1] However, despite the great success of OSC development to power conversion efficiencies (PCE) up to 19%^[2], there is still untapped potential for further improvement. One limiting factor is the total voltage loss ($\Delta V_{\text{loss}} = q^{-1}E_g - V_{\text{OC}}$), defined as the difference between the optical band gap (E_g) and the open-circuit voltage (V_{OC}).^[3-6] Thereby, ΔV_{loss} is composed of losses due to radiative (ΔV_r) and non-radiative (ΔV_{nr}) recombination.^[4, 7] According to the Shockley-Queisser limit, an ideal solar cell possesses only radiative recombination, making the contribution ΔV_r unavoidable.^[8, 9] Non-radiative recombination processes thus reduce V_{OC} and the short-circuit current and are therefore of great interest for OSC research.^[3, 5] Furthermore, after optical excitation of donor (D) or acceptor (A) moieties, charge transfer (CT) at the interface is expected to reduce the photovoltage due to the difference in the D or A band gaps and the energy of CT states ($E_g - E_{\text{CT}}$).^[6, 10, 11] However, in state-of-the-art D:A combinations, such as PM6:Y6, this difference is almost negligible, making non-radiative recombination the most dominant in terms of efficiency losses.^[7] Due to the close energetic alignment between NFA singlet states and the CT states, especially in the PBDB-T:Y-series blends, NFA triplet states are energetically located below the CT states and represent a significant non-radiative decay channel for excitons.^[12] Preventing the population of these triplet states is extremely difficult, even in state-of-the-art blends as shown in this work. Direct intersystem crossing (ISC) from optically-excited donor or acceptor singlet states to molecular triplet states is one of the possible triplet formation mechanisms.^[13] The yield of this geminate pathway depends on the number of optically-generated singlet excitons not reaching the D:A interface within their exciton diffusion length to undergo CT.^[14] Another loss pathway is due to triplet CT states that relax spin-allowed to energetically lower molecular triplet states, also called electron or hole back transfer (EBT, HBT).^[3, 15] Thereby, HBT from CT states formed via non-geminate recombination was shown to have a considerable impact on V_{OC} reduction.^[3] All triplet formation mechanisms can lead to triplet excitons, which are localized on the lowest-lying molecular triplet states and thus increase non-radiative recombination.

In the present work, we set the focus on the impact of donor and acceptor halogenation on the formation of triplet excitons. Halogenation of, e.g. donor polymers can improve device efficiencies, as shown for fluorination and chlorination of PBDB-T to yield PM6 and PM7, respectively.^[16-18] Thereby, halogenation is beneficial in terms of PCE, since it stabilizes the highest occupied molecular orbital (HOMO) energy level, resulting in increased V_{OC} .^[16, 19] However, the question arises if the reduced HOMO offset impacts the driving force of the, in NFA blends, important hole transfer (HT). Another advantage of halogenation is observed for morphology, since halogenation increases the molecular

planarity and ordering. This in turn results in improved aggregation, leading to a rise in charge carrier mobility and in fill factor.^[20] However, aggregation could lead to undissociated singlet excitons that undergo ISC. Additionally, ISC rates of organic semiconductors could be enhanced substantially by halogenation as shown for organic light-emitting diodes (OLEDs) employing thermally activated delayed fluorescence (TADF), where bromination or iodination increases reverse ISC rates due to the heavy atom effect.^[19] In this context, it remains to be clarified whether fluorination and chlorination of OPV materials also have an impact on ISC and HT kinetics or overall on triplet exciton formation.

Since formation of long-lived triplet states results in a loss of OSC performance and can exacerbate device degradation, studying the presence of triplet excitons and their generation mechanisms is essential. We used two complementary methods, which are highly sensitive to triplet excitons: photoluminescence detected magnetic resonance (PLDMR) and transient electron paramagnetic resonance (trEPR). Both methods were often applied independently of each other in the past to investigate triplet formation in OSCs.^[3, 21-24] Especially the combination of both techniques has recently been shown to be very powerful^[25]: trEPR probes triplet excitons directly by detection of microwave absorption between triplet sublevels occurring during resonance transitions and reveals highly spin polarized, i.e. geminate triplet exciton formation pathways, such as ISC or geminate HBT. In contrast, PLDMR probes triplet states indirectly with the higher sensitivity of optical detection and thus reveals those spin states that are associated with luminescence, e.g. via triplet-triplet annihilation (TTA), ground state depletion or (reverse) ISC.^[26, 27] PLDMR is therefore well-suited to detect long-lived triplet excitons including those formed by non-geminate recombination and identify their molecular localization.^[22, 23] To further study the influence of halogenation on excited state kinetics, including HT and ISC rates, we performed transient absorption (TA) measurements and quantum-chemical (QC) calculations. By the combination of these complementary techniques, we thoroughly investigated the photophysics of state-of-the-art donor and acceptor materials in different combinations: the polymer PBDB-T and its fluorinated and chlorinated variants, PM6 and PM7, as well as the halogenated NFAs Y6 and Y7 (Figure 1, whereby Y5 is used for comparison of (non-) halogenation in QC calculations).

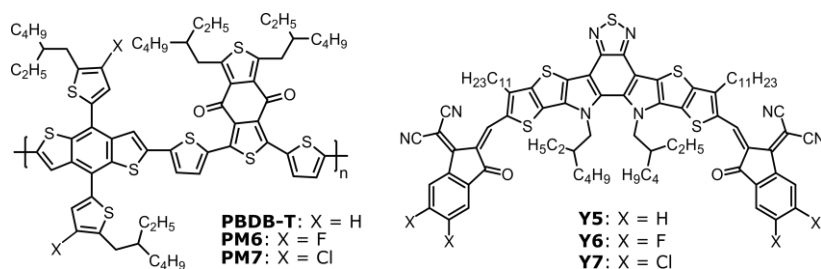


Figure 1. Chemical structures of studied organic solar cell materials. As donors PBDB-T (X = H), fluorinated version PM6 (X = F, also called PBDB-T-2F) and chlorinated version PM7 (X = Cl, also called PBDB-T-2Cl) are investigated. Acceptors represent Y5 (X = H, also called BTP), Y6 (X = F, also called BTP-4F) and chlorinated version Y7 (X = Cl, also called BTP-4Cl).

Probing Triplet Excitons with Magnetic Resonance

Triplet excitons (either CT or molecular) are characterized by two interacting electron spins, whose fundamental spin physics is briefly described in the following. The corresponding Hamiltonian operator in X-band regime (microwave frequency $\nu_{MW} \approx 9.4$ GHz and external magnetic field $B_0 \approx 340$ mT) can be reduced to mainly three contributions: the electron Zeeman (EZ) interaction \hat{H}_{EZ} , zero-field splitting (ZFS) \hat{H}_{ZFS} and exchange interaction \hat{H}_{EX} (other contributions, including hyperfine fields, can be considered as negligible perturbations):^[28]

$$\hat{H} = \hat{H}_{EZ} + \hat{H}_{ZFS} + \hat{H}_{EX} = \mathbf{g} \mu_B \hat{\mathbf{S}} \vec{B} + \hat{\mathbf{S}}^T \mathbf{D} \hat{\mathbf{S}} + \hat{\mathbf{S}}_1^T \mathbf{J} \hat{\mathbf{S}}_2$$

Here, $\hat{\mathbf{S}}$ is the total spin angular momentum operator (with $\hat{\mathbf{S}}_1$ and $\hat{\mathbf{S}}_2$ being the operators for the respective electron spins), \mathbf{g} the g -tensor (assumed to be isotropic due to a small spin-orbit coupling (SOC) in organic molecules) and μ_B the Bohr magneton, \mathbf{D} the ZFS tensor and \mathbf{J} the exchange-interaction tensor. The Zeeman interaction describes the quantized splitting of the paramagnetic states into their sublevels with spin quantum numbers $m_s = +1, 0, -1$, i.e. the spin Hamiltonian eigenstates $|T_-\rangle$, $|T_0\rangle$ and $|T_+\rangle$, based on the interaction with the external magnetic field \vec{B} .^[29] For nearby electron and hole (i.e. a locally excited state on a given molecule), the triplet sublevels are already energetically split in absence of an external magnetic field due to dipolar interactions between the spins of the unpaired electrons. This splitting is referred to as ZFS with the two scalar parameters D and E of the corresponding ZFS tensor \mathbf{D} : the axial parameter D is related to the average inter-spin distance r (to first order approximation $D \sim r^{-3}$), whereby E describes the rhombicity, thus the deviation from axial symmetry.^[28, 30, 31] For CT states with larger spin-spin distances than those of molecular states, spin conservation during charge separation generates spin-correlated radical pairs (SCRPs) with exchange J and dipolar interaction D being in a comparable range. The Hamiltonian eigenstates are then represented by pure $|^3CT_-\rangle$ and $|^3CT_+\rangle$ triplet states ($m_s = \pm 1$) and two mixed singlet-triplet states $|^3CT_0\rangle$ and $|^1CT_0\rangle$ ($m_s = 0$), whereby due to angular momentum conservation, only a spin mixing between the latter two can occur. Further information about triplet spin states is given in SI.

1. Detecting Triplet Excitons with Spin-Sensitive Photoluminescence

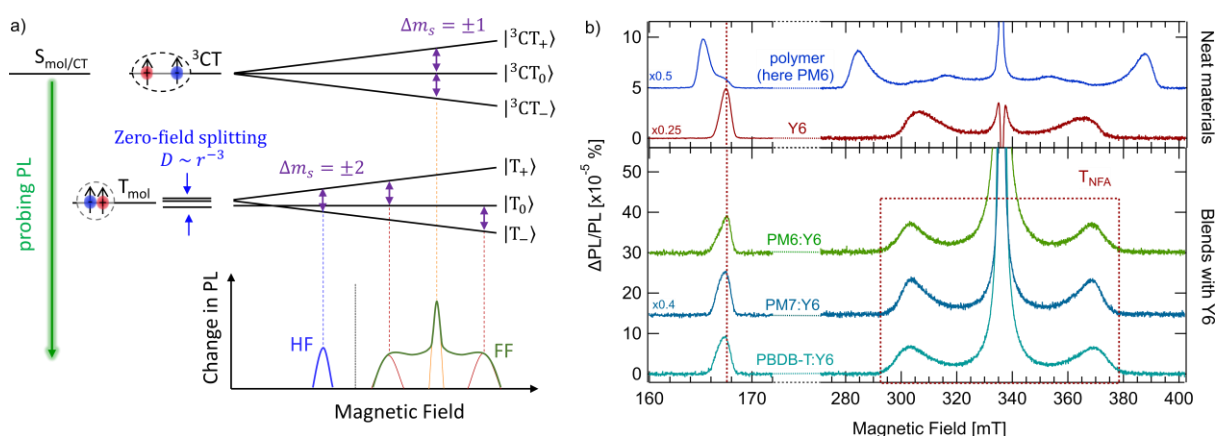


Figure 2. Photoluminescence detected magnetic resonance (PLDMR) of triplet excitons. a) PLDMR probes PL changes of singlet states ($S_{\text{mol/CT}}$), which are coupled to paramagnetic triplet states. CT and molecular triplet states (${}^3\text{CT}$, T_{mol}) are split due to Zeeman interaction and the ZFS parameter D : $|{}^3\text{CT}_{+,0,-}\rangle$, $|T_{+,0,-}\rangle$. Microwave irradiation induces $\Delta m_s = \pm 1$ transitions (purple), leading to a change in the PL yield detected as full field spectrum (FF). An additional signal is detected at half the magnetic field (HF) for $\Delta m_s = \pm 2$ transitions. b) PLDMR spectra for the neat materials PM6 and Y6 are shown together with the blends PBDB-T:Y6, PM6:Y6 and PM7:Y6. The spectral width of the FF signal and the position of the HF signal are determined by the material-dependent ZFS and therefore the triplet excitons in the blends can be assigned to the NFA Y6 (red dotted box). All PLDMR measurements used $\lambda_{\text{ex}} = 473$ nm for excitation of donor and acceptor and were performed at $T = 10$ K.

Figure 2a depicts the PLDMR principle of probing the PL change of singlet states (either CT or molecular), which are coupled (via TTA, ISC, etc.) with paramagnetic states.^[24] Microwave irradiation induces transitions between the sublevels (purple arrows) leading to a change in PL intensity. In the case of ${}^3\text{CT}$ states, the comparatively large inter-spin distance results in negligible dipolar interaction (negligible D value), which in turn induces a symmetrical splitting of triplet sublevels $|{}^3\text{CT}_{+}\rangle$, $|{}^3\text{CT}_{0}\rangle$ and $|{}^3\text{CT}_{-}\rangle$ in a magnetic field. Microwave irradiation of frequency ν_{MW} , resonant to the energetic sublevel splitting, induces spin-allowed $\Delta m_s = \pm 1$ transitions at closely spaced magnetic field values. The result is a change of steady-state triplet population, leading to an increased ($\Delta\text{PL}/\text{PL} > 0$) or reduced ($\Delta\text{PL}/\text{PL} < 0$) PL yield under resonance conditions, referred to as full-field (FF) signal. For the case of a localized molecular triplet (T_{mol} in Figure 2a), the ZFS results in an asymmetric splitting of the triplet sublevels in the applied magnetic field. Thus, microwave irradiation induces transitions and PL changes at more widely spaced magnetic field values, the distance of which depends linearly on the ZFS parameters D and E , as further addressed below. In addition, there is a certain probability of $\Delta m_s = \pm 2$ transitions at half of the resonant magnetic field, referred to as half-field (HF) signal.^[30] The intensity of the HF signal increases quadratically with D (intensity $\sim D^2 \sim r^{-6}$) and is therefore detectable for molecular triplet excitons only.^[32] The total width of the spectrum in magnetic field units ($|2D|/g\mu_B$) together with the spectral position of the HF spectrum allows for the molecular localization of the triplet states involved in the PL generation process to be readily determined.^[23]

Figure 2b presents PLDMR spectra of the pristine materials PM6 and Y6 as well as blends of Y6 with the polymer donors PBDB-T, PM6 and PM7. The measurements were performed for thin-film samples produced by an optimized spin-coating recipe comparable to OSC device production (recipe given in Experimental Section, measurements for drop-cast samples in EPR tubes are shown in Figs. S9 and S10).^[33, 34] The PLDMR spectra of the pristine polymers are almost identical; PM6 is shown here while the spectra of PBDB-T and PM7 can be found in Figure S8. All polymer spectra show a broad molecular triplet feature of 110 mT width ($D/h = 1500$ MHz) and a HF signal at $B = 165$ mT. Pristine NFA Y6 shows a molecular triplet signal with a smaller width of 70 mT, corresponding to $D/h = 940$ MHz and a HF signal at $B = 166.8$ mT. Spectral simulation parameters derived by the MATLAB toolbox EasySpin^[35] are summarized in Table S5. PLDMR spectra of all materials show additional central narrow peaks, which have previously been assigned to spontaneously separated charge carriers, also called polaron pairs (PP) with a weak dipolar interaction.^[23, 36, 37] When blending Y6 with the donors PM6, PM7 and PBDB-T (lower traces), the intensity of the central peak increases significantly due to the increased formation of separated polaron pairs, spectrally overlapping with D:A interfacial CT states. Since PLDMR is performed on thin films without electrodes, all formed CT states and polaron pairs do eventually recombine. We previously showed that the CT peak in PLDMR PM6:NFA blends has a positive sign^[22], which is assigned to triplet-polaron annihilation (TPA), being a central bimolecular interaction in these OSC.^[3, 37, 38]

All three blends show a broad triplet feature (300 – 370 mT) arising from long-lived molecular triplet excitons. The D value, i.e. the width of the FF spectra, and the positions of the HF signals at 166.8 mT (dotted vertical line) clearly assign these PLDMR features to triplet excitons on the NFA Y6. The D value in the blends is slightly larger with $D/h = 1020 - 1040$ MHz (Table S5) than in neat Y6 due to a marginally different molecular packing. However, the spin density delocalization is not strongly affected according to the relation $D \sim r^{-3}$. Furthermore, the triplet features in all PLDMR spectra can only be simulated taking considerable molecular ordering into account, leading to pronounced spectral “wings”.^[35, 39] The ordering factor λ gives information about the preferential orientation of the molecules, whereby θ is the angle between the molecular z-axis and the applied magnetic field. In neat Y6, the ordering factor of $\lambda_\theta = 3.8$ corresponds to a preferential orientation of the molecules in direction of the applied magnetic field, in line with face-on stacking of Y6 with respect to the substrate and enhanced crystallinity found for samples from chloroform (CF) solutions.^[40-42] When blending Y6 with the polymers, the ordering is maintained with slightly increased values ($\lambda_\theta = 4.2$ for PBDB-T:Y6 to $\lambda_\theta = 5.5$ for PM6:Y6 and PM7:Y6). The similar ordering factor in the blends supports that the backbone ordering known for neat Y6 remains present in the blends, as already confirmed for PM6:Y6 by GIWAXS measurements in literature.^[43] The PLDMR spectra also suggest similar preferential orientation of Y6

in PBDB-T:Y6 and PM7:Y6, whereby this face-on orientation in the blend is shown to be beneficial for charge transport in the direction normal to the substrate surface.^[44, 45]

The triplet excitons detected on the NFA can be generated either by direct ISC, non-geminate HBT or by geminate HBT. Although PLDMR is not able to distinguish between these pathways, its high sensitivity is crucial to reveal the presence of all long-lived triplet excitons. This sensitivity is achieved due to the optical detection and the continuous illumination, enhancing spin polarization due to annihilation effects, i.e. TTA in molecular triplet features, as discussed in more detail below.^[25] PLDMR measurements were also performed with NFA Y7 (Figure S10), where long-lived triplet excitons were found on Y7. Hence, we observe molecular triplet excitons in all studied OPV blend, localized on the NFA.

2. Probing Triplet Pathways with Transient EPR

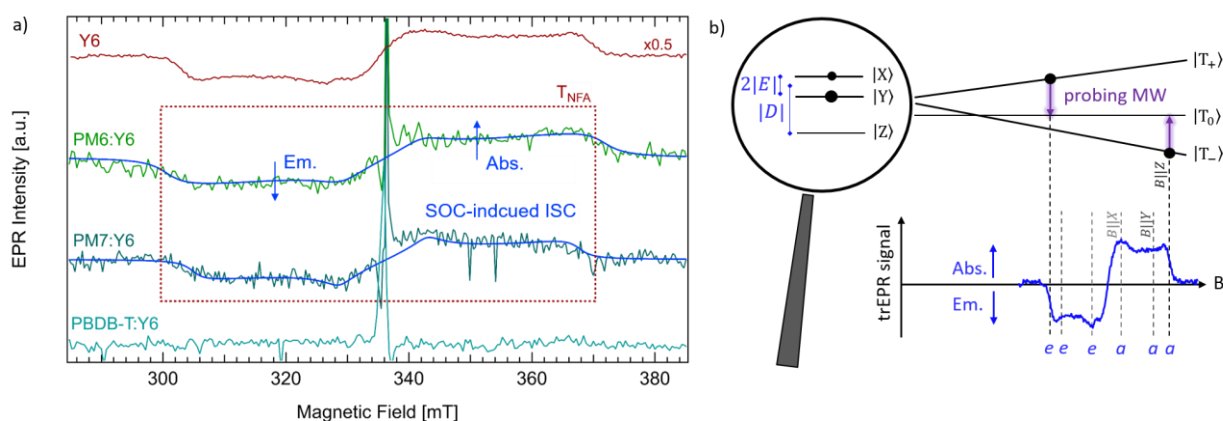


Figure 3. trEPR spectra of pristine Y6, PM6:Y6, PM7:Y6 and PBDB-T:Y6. a) trEPR spectra of blends with the halogenated donors (PM6 and PM7) have the same spectral fingerprint as triplets on pristine Y6 (red dotted box) as shown by the spectral fits (blue). The blend of PBDB-T:Y6 shows no detectable triplet formation. b) Formation of polarized trEPR spectra for spin-orbit coupling (SOC) driven ISC triplets. ISC is sublevel selective and acts on the zero-field sublevels $|X\rangle$, $|Y\rangle$ and $|Z\rangle$. These populations are converted into high-field populations $|T_+\rangle$, $|T_0\rangle$ and $|T_-\rangle$, depending on the three principal axes orientation of the ZFS tensor \mathbf{D} with respect to magnetic field \vec{B} . Microwave emission (e) or absorption (a) for $\Delta m_s = \pm 1$ transitions (purple) results in the shown Y6 trEPR pattern (blue). The $eeaaa$ polarization pattern is due to SOC-driven ISC. All trEPR measurements used $\lambda_{ex} = 532$ nm for excitation of donor and acceptor and were performed at $T = 10$ K.

While PLDMR probes steady-state populations due to continuous illumination, trEPR probes short-lived spin polarization generated by pulsed laser excitation. Thereby, trEPR is able to reveal generation pathways of geminate triplet excitons with distinct spin-polarization due to specific mechanisms, such as triplet states populated by ISC.^[29, 30] As discussed below, the fraction of these geminate triplet excitons is very low in the studied blends. For the spin-coated samples, this yields a signal that is detectable but too weak to determine the spin polarization pattern with confidence (Figure S2).

Therefore, trEPR measurements were additionally performed on drop-cast samples (Figure 3), which yielded a better signal-to-noise ratio to reliably identify the population mechanism (see SI).

Figure 3a shows the trEPR spectrum of Y6 and its blends with the three donor polymers (trEPR of pristine polymer donor as well as blends with Y7 are shown in Figure S13 and Figure S14). Neat Y6 shows a 70 mT wide spectrum, corresponding to $D/h = 945$ MHz, similar to the value obtained with PLDMR ($D/h = 940$ MHz). When blending Y6 with the polymers, all blends show an additional intense CT signal with narrow microwave emission/absorption feature ($B = 336.5$ mT), corresponding to a SCRP. The width correlates with that of PLDMR CT/PP features in Figure 2b, assigning both to the same ^3CT states. Regarding the molecular (broad) trEPR feature, almost identical spectral fingerprints are detected for the blends of PM6:Y6 and PM7:Y6. The same spectral width proves that this signal is also arising from Y6 triplet excitons as already shown with PLDMR. In contrast to PLDMR, trEPR spectra can be simulated without considering molecular ordering.^[25] This is attributable to the fact that trEPR probes all (highly) spin-polarized triplet excitons, while PLDMR probes predominantly those triplets that are associated with luminescence, e.g. via more dominant TTA in crystalline phases due to an increased diffusion length.^[25, 46, 47] The polarization pattern of the trEPR signal of PM6:Y6 and PM7:Y6 displays microwave emission at lower fields and microwave absorption at higher fields, consistent with triplet excitons populated by SOC-driven ISC, i.e. geminate pathway.

Regarding PBDB-T:Y6, molecular triplet excitons on Y6 are detected with PLDMR (Figure 2b), whereby no molecular triplet feature in trEPR is observed. While trEPR only probes geminate triplet excitons, PLDMR is also sensitive to triplet excitons formed by non-geminate recombination. This finding assigns the triplet excitons in PBDB-T:Y6 visible in PLDMR (Figure 2) to non-geminate HBT. As also discussed below, non-geminate triplet excitons represent the main contribution of energetically trapped triplet excitons. Thus, the triplet yield visible in trEPR is overall a very minor triplet channel but important to proof the mechanism of SOC-driven ISC.

Figure 3b shows the formation of the trEPR spectral pattern of the spin-polarized triplet feature of the neat materials and the blends. It arises by the selective population of the triplet sublevels by ISC from the excited singlet states.^[30] This ISC mechanism for molecular excitons with small wave function extent (large D value) is based on SOC, which is dominant for small electron-hole distances.^[48] At larger inter-spin distances, SOC is negligible and (reverse) ISC is driven by hyperfine interactions (HFI) leading to different trEPR spectral patterns for, e.g. triplet excitons formed via geminate HBT, discussed further in the SI.^[3, 49] SOC-driven ISC acts on the zero-field triplet states, given by the eigenstates $|X\rangle$, $|Y\rangle$ and $|Z\rangle$ of the Hamiltonian (where X, Y and Z are the principal axes of the ZFS tensor \mathbf{D}), which are split due the ZFS parameters D and E .^[28, 29] The ISC rate depends on the difference in the nature of the singlet and triplet excited states involved in this process, whereby the population is spin selective, depending

on the symmetries of the excited singlet and triplet wave functions.^[29, 30, 50, 51] In the studied materials, SOC-driven ISC leads to a relative population p_i of zero-field triplet sublevels, in, e.g. neat Y6 of $[p_z, p_y, p_x] = [0, 0.66, 0.34]$ (see Section 6 and Table S7 in SI). In a magnetic field, the population of the corresponding high-field sublevels $|T_+\rangle, |T_0\rangle, |T_-\rangle$ can be derived from the zero-field population, which depends on the orientation of the ZFS tensor with respect to the external magnetic field (here shown for $\vec{B}||Z$, further details in Figure S11).^[29] In this projection, the $|T_+\rangle$ and $|T_-\rangle$ states are more populated than $|T_0\rangle$, with resonant microwave irradiation driving this imbalance towards equal distributions. Together with the asymmetric splitting due to ZFS, microwave emission (e) at lower fields (negative intensity) and enhanced absorption (a) at higher fields (positive intensity) can be detected with trEPR.^[30] In disordered organic samples, transitions from all orientations of \mathbf{D} with respect to \vec{B} are superimposed as a characteristic spectrum with $eeaaa$ pattern, which is indicative for triplet excitons populated by SOC-driven ISC (Figure S11).^[29] Returning to Figure 2a, the SOC-driven ISC pattern of Y6 triplets is also present in the blends of PM6:Y6 and PM7:Y6 with similar zero-field population of triplet sublevels as neat Y6 (Table S7), indicating ISC on the NFA, as further discussed below.

Influence of Halogenation on Excited State Kinetics

1. Hole Transfer in (Non-) Halogenated PBDB-T:Y-Series studied by Transient Absorption

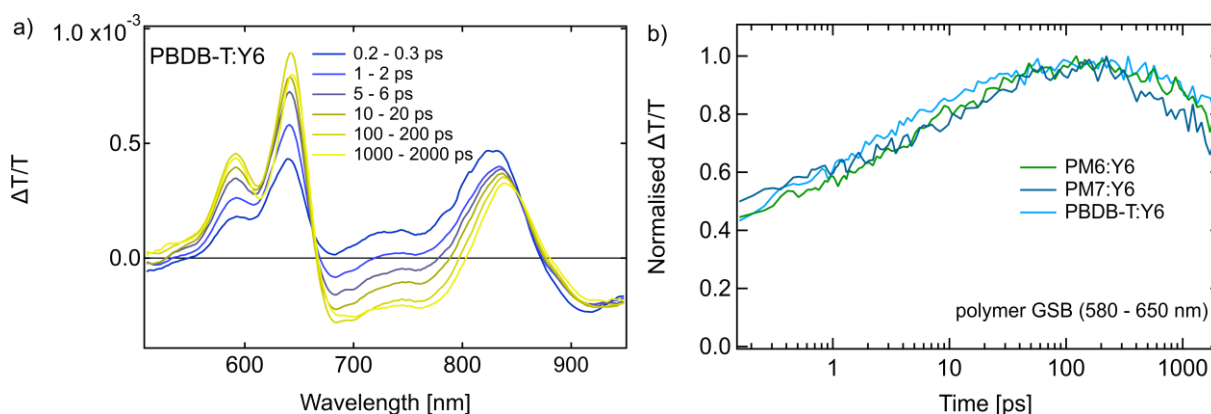


Figure 4. Transient absorption (TA) measurements. a) TA spectra at different time delays for PBDB-T:Y6. b) HT kinetics extracted from polymer ground state bleach GSB (580 – 650 nm) for PM6:Y6, PM7:Y6 and PBDB-T:Y6. In all samples, HT takes place on comparable timescales. All TA measurements used a pump pulse wavelength of 800 nm for selective excitation of Y6 and were performed at $T = 293$ K.

Figure 4 shows transient absorption (TA) spectra and HT kinetics for Y6 blends with excitation wavelength of 800 nm for selective excitation of the NFA Y6 (blends with Y7 shown in Figure S3). The low fluence of $\sim 0.6 \mu\text{J cm}^{-2}$ used in the TA measurements on the blends prevents excess bimolecular recombination in the first few nanoseconds from affecting the determination of the HT timescales.

Figure 4a shows the time dependent TA spectra of PBDB-T:Y6; TA spectra for PM6:Y6 and PM7:Y6 are shown in Figure S1. The Y6 ground state bleach (GSB) centered at 830 nm and photo-induced absorption (PIA) of Y6 singlet excitons at 910 nm are observed immediately after optical excitation.^[52, 53] In addition, a clear GSB at 580 - 650 nm emerges in the TA spectra, consistent with the absorption spectrum of the polymer.^[54, 55] Since the excitation pump does not generate excitons on PBDB-T (PM6, PM7 respectively), the appearance of the polymer GSB indicates dissociation of Y6 excitons via HT at the D:A interface. The presence of the polymer GSB already at 0.2 ps in all blends suggests that some ultrafast HT occurs.^[52, 56] However, as the Y6 GSB falls, likely due to some spectral overlap with the negative sign PIAs of Y6 electron and PM6 hole polarons forming at 780 nm and 920 nm^[57], respectively, the polymer GSB continues to increase, peaking around 100 ps. This indicates that a significant population of the NFA excitons require additional time to dissociate. On similar timescales, another broad negative band grows in between 680 and 730 nm. This has previously been assigned to the electro-absorption of the donor polymer PM6, indicating the separation of bound interfacial CT states into free charges.^[3, 52, 57] All blends with NFA Y6 show a considerable HT yield, whilst it decreases upon halogenation of the donor in these blends (Figure S1) and with NFA Y7 (Figure S3), further discussed below and in Sections 2 and 3 of SI.

Figure 4b shows the normalized HT kinetics from the polymer GSB between 580 and 650 nm. The HT rate appears to be comparable for all donor combinations (PBDB-T, PM6 and PM7) with Y6. In addition to the ultrafast component already visible at 0.2 ps, the HT yield increases up to a peak at 100 ps, indicating that the HT is completed. Donor combinations with NFA Y7 (Figure S3) also show very similar HT kinetics to Y6 blends. The slower HT rate component is often attributed to diffusion limitations for excitons created far from the D:A interface.^[58, 59] Zhong *et al.* performed measurements on 5:1 polymer:NFA blends to disentangle the ultrafast component, determined by intrinsic CT rates, from the morphology dependent exciton diffusion rates.^[56] However, the studied blends show similar kinetics in both components, reflecting that neither the small energetic shift in HOMO level (Figure S15) nor probable morphology differences upon halogenation have a significant impact on the HT rates, which has been found to be largely governed by the interfacial morphology in PM6:Y6.^[52] However, despite initially generating a similar number of excitations on Y6 (as seen by the equal intensity of the Y6 GSB at 0.2 ps in all blends), the intensity of the polymer GSB reaches the highest value in PBDB-T, followed by PM6 and then PM7 (Figure S1). This indicates a difference in the absolute HT yield, implying that a smaller number of Y6 excitons reaches the D:A interface for HT, e.g. due to larger domain sizes involving halogenated donors, as further discussed below.

2. SOC-driven ISC in (Non-) Halogenated Y-Series by Quantum-Chemical Calculations

Singlet excitons formed upon photoexcitation which do not reach the D:A interface for efficient HT may eventually undergo ISC to the respective triplet states. We performed QC calculations to assess possible differences in the ISC rates due to halogenation. In the assessment of the energetic landscape of the investigated donor polymers and the NFA Y-series, singlet and triplet vertical excitation energies were computed by means of *screened* range-separated hybrid (SRSH) time-dependent DFT calculations, performed within the Tamm-Dancoff approximation (TDA) (see SI for further details and Table S2).^[60, 61] In order to obtain triplet energies, the theoretical singlet-triplet energy gap ΔE_{ST} was subtracted from experimental singlet energies (Table S2). Then, we focused on the calculation of ISC rates k_{ISC} for the NFA Y-series and we resorted to the semi-classical Marcus-Levich-Jortner expression, which treats high-frequency intramolecular vibrational modes in a quantum-mechanical fashion:

$$k_{ISC} = \frac{2\pi}{\hbar} |\langle T_x | \hat{H}_{SOC} | S_1 \rangle|^2 \sqrt{\frac{1}{4\pi\lambda_s k_B T}} \times \sum_n \left\{ \exp(-S) \frac{S^n}{n!} \times \exp \left[-\frac{(-\Delta E_{S_1-T_x}^0 + \lambda_s + n\hbar\omega)^2}{4\lambda_s k_B T} \right] \right\}$$

Here, $|\langle T_x | \hat{H}_{SOC} | S_1 \rangle|$ displays the SOC matrix element involved in the ISC process from S_1 to the manifold of the triplet states T_x , whose energy differences were given by $\Delta E_{S_1-T_x}^0$; λ_s is the external reorganization energy (set in a range between 0.05 and 0.2 eV); \hbar is the reduced Planck's constant; k_B is the Boltzmann constant; and T is the temperature (set at 298 K). $\hbar\omega$ is the energy of an effective high-frequency intramolecular vibrational mode (0.15 eV of a carbon-carbon stretching) that assists the ISC and $S = \lambda_i/(\hbar\omega)$ is the Huang-Rhys factor, which is a measure of the electron-phonon coupling assisting the ISC process and λ_i the internal reorganization energy.

The nature of S_1 excited state of Y6 and Y7 is very similar to that of T_1 excited state which makes SOC between these excited states negligible according to the El-Sayed's rule.^[62, 63] For instance, in Y6 both S_1 and T_1 show a dominant HOMO-to-LUMO transition (98% for S_1 and 90% for T_1 , in agreement with literature^[64], see Figure S6) leading to a very small SOC value ($< 0.05 \text{ cm}^{-1}$). In contrast, the T_2 excited state (which is energetically also below S_1) shows a contribution of 75% of HOMO-to-LUMO+1 transition, involving a different localization of the electron wave function (see Figure S6) in comparison to S_1 . Consequently, SOC between S_1 and T_2 is much larger (on the order 0.1 cm^{-1}) compared to the SOC between S_1 and T_1 , enabling singlet-triplet conversion by ISC on the NFAs.

Moreover, to study the influence of halogenation, we compared Y6 and Y7 together with the non-halogenated version Y5. The same natural transition orbitals (NTOs) were found in all three cases, meaning that the relevant low-lying excited states (namely S_1 and T_2) has the very same nature and halogenation does not play a key role here. In fact, the electron density on the halogen atoms in the

NTO is negligible (Figure S6), resulting in the SOC matrix element being almost insensitive to halogenation. As the respective ΔE_{ST} is also not changing considerably (Table S2) and, additionally, has been shown to have a minor influence on the ISC rate, the SOC-driven ISC kinetics from S_1 via T_2 can be assumed to be comparable for all (non-) halogenated acceptors.

Discussion

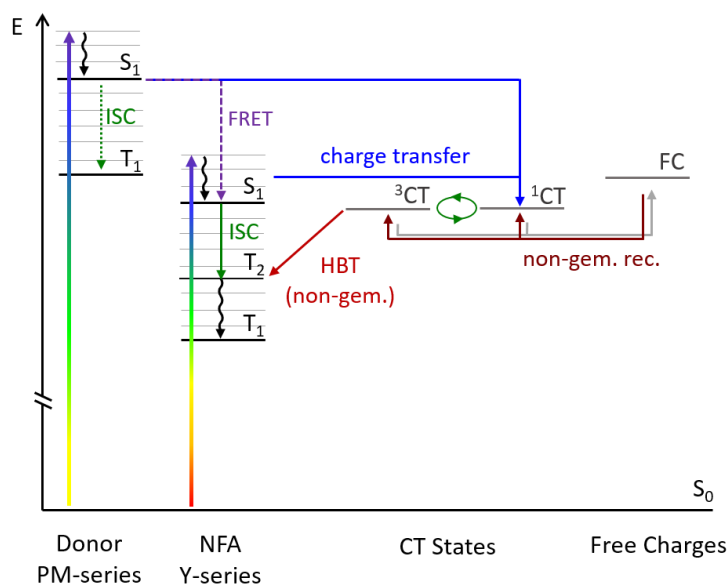


Figure 5. Energy diagram of the studied OPV blends. Optical excitation of donor or acceptor singlet is followed by interfacial charge transfer, FRET or direct ISC. NFA triplet states (T_1 , T_2) are energetically below the intermolecular CT states (3CT , 1CT) and therefore represents energetic trap states. NFA triplet states are occupied by ISC from the NFA S_1 state or by HBT from 3CT , which itself is populated by non-geminate recombination of free charges (FC). PL emission arrows from S_1 and 1CT states are omitted for clarity.

Figure 5 shows the Jablonski diagram of the studied PBDB-T:Y-series blends. All energies and observed triplet formation mechanisms are summarized in Table S1. The investigated NFAs possess a low-lying singlet state with a small offset to the CT energy, allowing small energy losses in comparison to fullerene-based solar cells, but resulting in the lowest NFA triplet being energetically below the CT states.^[5, 53] Given the large ΔE_{ST} of molecular states ($\approx 0.5 - 0.6$ eV), NFA triplet excitons are not able to undergo interfacial CT and do not yield photocurrent, but instead are energetically trapped. Triplet excitons have small non-radiative decay rates and are long-lived, thus detectable with both PLDMR and trEPR.^[3, 25] In the following, we discuss the different pathways affecting the population of the triplet states (direct ISC from S_1 states upon photo-excitation as well as HBT from triplet CT states formed via either geminate or non-geminate recombination) and the impact of halogenation on the overall photophysics, e.g. ISC or HT rates.

1. Triplet Formation by Geminate Pathways

Triplet excitons are detected in all PBDB-T:Y-series blends on the NFA triplet states (Figure 2 and Section 5 in SI). The polarization patterns in trEPR (Figure 3) are consistent with polarization for SOC-driven ISC triplets (*eeaaaa*). These direct ISC-driven triplet states can be clearly distinguished from other triplet formation processes, such as HBT from triplet CT states formed via geminate recombination as observed to be a dominant process in polymer:fullerene blends.^[14, 25] However, in the investigated NFA-based blends, no indication of geminate HBT could be observed, ruling out this triplet formation mechanism, as also reported in literature.^[3] The comparable zero-field populations of the blends and neat Y6 (see Section 6 and Table S7 in SI) indicate that ISC takes place on the NFA, e.g. in the center of NFA domains larger than the exciton diffusion length away from the D:A interface. The SOC-driven ISC is additionally increased by the presence of higher-lying triplet states with larger variation in their nature with respect to S_1 , increasing the SOC matrix element. As for the donor, ultrafast electron transfer quenches the singlet excitation in the sub-picosecond timescale, with the possibility of Förster resonance energy transfer (FRET) to the NFA as another deactivation channel in these blends.^[11, 52, 59, 65] Thus, the fast depopulation of the donor singlet states is kinetically outcompeting slower ISC on the polymers, suggesting the yield of excitons undergoing ISC to be negligible (dotted arrow in Figure 5). Even if donor triplet states were populated with low yield, they would still be energetically above the CT and NFA states and could undergo charge or Dexter energy transfer. Thus, triplet excitons on the polymer donor are not energetically trapped in these blends and do not have to be considered as an efficient loss channel.

2. Triplet Formation by Non-Geminate Pathways

The NFA triplet yield in OSCs by SOC-driven ISC is assumed to be low, as evidenced by a weak trEPR signal for spin-coated substrates (Figure S2). We additionally confirmed HBT from triplet CT states formed via non-geminate recombination of free charge carriers, visible in all PLDMR spectra. The recombination of free charge carriers with uncorrelated spin orientation will lead to the formation of 25% CT singlets and 75% CT triplets.^[66] The latter can relax spin-allowed to the lowest molecular triplet states via non-geminate HBT (dark red arrows in Figure 5).^[15] Thereby, excitons initially occupy the three triplet sublevels equally due to spin statistics but form within the spin-lattice relaxation time τ , in X-band regime, weak spin polarization according to Boltzmann statistics. Additionally, continuous optical excitation, as in PLDMR, enhances the spin polarization due to accumulation of triplet excitons and subsequent spin-dependent annihilation processes. In combination with the optical detection, this method proves to be very sensitive to non-geminate triplet excitons. Thus, trEPR alone could miss triplet excitons despite their significant presence as for the example of PBDB-T:Y6. Gillett *et al.* showed with TA spectroscopy that in the blend PM6:Y6 around 90% of the non-geminately recombined CT

states undergo HBT to the NFA triplet.^[3] In contrast, the ISC yield in neat Y6 is around 3%, further reduced in the blends due to a significant CT of 90% of the generated excitons.^[3] Regarding the similarity of ISC and HT rates discussed below, we assume a similar amount of triplet excitons in all PBDB-T:Y-series blends from non-geminate recombination, detectable in all blends via PLDMR (Figure 2). Since the rate of non-geminate HBT is shown to increase with temperature, the presence of non-geminate HBT triplet excitons even at 10 K highlights the importance of this loss channel for solar cells operated at ambient temperatures.^[3]

3. Excited State Kinetics of ISC and HT

As the yield of excitons undergoing the above-mentioned processes depends on the kinetics of the system, we discuss in the following the two most important rates affecting the population of triplet states upon excitation of the singlet states: HT and ISC rates. As differences in HT kinetics would give the singlet excitons more/less time to undergo ISC, we studied the impact of halogenation on these rates. Regarding the halogenation of the acceptor, one could invoke an increase in SOC due to heavier halogen atoms. These circumstances would boost ISC and change the overall excited states kinetics, as has already been shown in literature for bromine or iodine in TADF molecules.^[67] However, QC calculations on NFA Y-series reveal that, starting from the non-halogenated acceptor Y5, the ISC rate does not change significantly upon fluorination and chlorination in these molecules due to the absence of significant weight on the halogen atoms (see Table S3, Figure S6 and Figure S7 for the donor polymer PM6). As for the HT kinetics, halogenation of PBDB-T lowers the donor HOMO energy level (Figure S15), leading to increased V_{oc} in solar cells with PM6 and PM7.^[54, 68] The smaller energy offset is desirable to minimize energy loss but one could consider an effect on the driving force due to a smaller HOMO offset.^[16, 59] However, TA measurements (Figure 4b) showed a comparable HT rate with the three different (non-) halogenated donors and with both NFAs (Figure S4). This outcome is not surprising, as the overall HT rate has been shown not being sensitive to the HOMO offset, especially in low-offset OSC: while the 'intrinsic' HT rate of NFA excitons generated in close proximity to the D:A interface occurs on sub-ps timescales, the overall HT process takes place over timescales of tens of picoseconds, depending on exciton diffusion in the bulk morphology.^[56] Furthermore, Ma *et al.* showed that HT rates for PM6:Y6 are only weakly affected by temperature in the range from 15 to 300 K, allowing the comparison with the low-temperature EPR measurements.^[65] Overall, the triplet population kinetics upon initial singlet excitation are shown to be comparable for (non-) halogenated donor and acceptor combinations.

4. Exciton Yields of ISC and HT

While the HT and ISC kinetics are comparable for all PBDB-T:Y-series blends, the yield of excitons undergoing these processes are determined to be different. The most probable reasons are due to

differences in the morphology or domain sizes, depending on halogenation of donor/acceptor and the choice of the solvent. We fabricated all spin-coated samples with the optimized recipe for PM6:Y6, dissolved in CF (see Experimental Section).^[34, 69] However, we note that the HT yield decreases significantly for PM6:Y6 when changing from CF to chlorobenzene (CB) as solvent, in contrast to PM6:Y7, where the HT yield remains comparable in both blends (Figure S5), suggesting a strong influence of morphology on HT yield. Also Eastham *et al.* investigated different donor materials with NFA ITIC, demonstrating that efficient HT depends strongly on the blend morphology rather than the energy level alignment.^[70] While the used recipe is optimized for acceptor Y6, the literature suggests that better device performance for chlorinated acceptors, e.g. PM6:Y7, is obtained with CB, as further discussed in Section 3 of SI.^[33, 71] Comparing TA and trEPR for Y6 blends with substrates prepared in the same way according to the optimized recipe (Figure S1 and Figure S2), the HT yield decreases upon halogenation, while trEPR data show a detectable ISC yield in PM6:Y6 and PM7:Y6. These results could stem from an increased size and purity of domains due to fluorination and chlorination^[69, 72, 73], e.g. due to reduced miscibility upon halogenation, decreasing the number of excitons reaching the D:A interface.^[72] However, domain sizes in the range of the exciton diffusion length are normally beneficial for dissociation of charge carriers, improving short-circuit current J_{sc} and fill factor FF of the solar cell.^[69, 72] Thus, the key point for a good performing OSC is matching a good trade-off in bulk morphology between efficient generation of charge transfer states and subsequent exciton dissociation.^[74] However, the higher efficiencies for PM6:Y6 and PM7:Y6 in comparison to PBDB-T:Y6 show that the positive impacts of halogen atoms, i.e. improved domain purity and higher V_{oc} upon halogenation of the donor, are more influential on solar cell performance.

Conclusion

In this work, we applied triplet spin-sensitive techniques (PLDMR, trEPR) together with TA and QC calculations to reveal loss processes by non-radiative triplet excitons. Using the strengths of these complementary methods, we were able to detect and distinguish all triplet excitons present in the investigated blends and draw a comprehensive picture of their generation pathways. We thereby studied different state-of-the-art donor:acceptor combinations with the (non-) halogenated polymers PBDB-T, PM6, PM7 and the NFAs Y6 and Y7 and detected long-lived triplet excitons in all blends. These excitons are energetically trapped on the low-lying NFA triplet state, where they are unable to contribute to OSC performance due to a high energetic gap to CT states. While the major contribution observed in all blends is non-geminate HBT, in blends with halogenated donors there is also a triplet population pathway through SOC-driven ISC on the NFA. The impact of halogenation on the rates affecting the population of triplet states after excitation of the NFA singlet states, in particular ISC and

HT, is comparable for all donor:acceptor combinations. Thus, shifting of HOMO levels or the presence of heavier halogen atoms have a minor influence on excited states kinetics. However, the increased triplet exciton yield by ISC with best performing PM6 and PM7 indicates an incomplete charge carrier generation, suggesting an adverse impact of domain aggregation through halogenation. While the benefits of halogenation still prevail in terms of overall device efficiency, the detection of energetically trapped triplet excitons in all these (non-) halogenated blends clearly shows that there is untapped potential to further improve plateauing OSC efficiencies.

Experimental Section

As donor materials, poly[[4,8-bis[5-(2-ethylhexyl)-2-thienyl]benzo[1,2-*b*:4,5-*b'*]dithiophene-2,6-diyl]-2,5-thiophenediyl[5,7-bis(2-ethylhexyl)-4,8-dioxo-4*H*,8*H*-benzo[1,2-*c*:4,5-*c'*]dithiophene-1,3-diyl]]polymer (PBDB-T), poly[[4,8-bis[5-(2-ethylhexyl)-4-fluoro-2-thienyl]benzo[1,2-*b*:4,5-*b'*]dithiophene-2,6-diyl]-2,5-thiophenediyl[5,7-bis(2-ethylhexyl)-4,8-dioxo-4*H*,8*H*-benzo[1,2-*c*:4,5-*c'*]dithiophene-1,3-diyl]-2,5-thiophenediyl] (PBDB-T-2F or PM6) and poly[[4,8-bis[5-(2-ethylhexyl)-4-chloro-2-thienyl]benzo[1,2-*b*:4,5-*b'*]dithiophene-2,6-diyl]-2,5-thiophenediyl[5,7-bis(2-ethylhexyl)-4,8-dioxo-4*H*,8*H*-benzo[1,2-*c*:4,5-*c'*]dithiophene-1,3-diyl]-2,5-thiophenediyl] (PBDB-T-2Cl or PM7) were used. NFAs represent 2,2'-((2*Z*,2'*Z*)-((12,13-bis(2-ethylhexyl)-3,9-diundecyl-12,13-dihydro-[1,2,5]thiadiazolo[3,4-*e*]thieno[2'',3'':4',5']thieno[2',3':4,5]pyrrolo[3,2-*g*]thieno[2',3':4,5]thieno[3,2-*b*]indole-2,10-diyl))bis(methanylylidene))bis(5,6-difluoro-3-oxo-2,3-dihydro-1*H*-indene-2,1-diylidene))dimalononitrile (BTP-4F or Y6) and 2,2'-((2*Z*,2'*Z*)-((12,13-bis(2-ethylhexyl)-3,9-diundecyl-12,13-dihydro-[1,2,5]thiadiazolo[3,4-*e*]thieno[2'',3'':4',5']thieno[2',3':4,5]pyrrolo[3,2-*g*]thieno[2',3':4,5]thieno[3,2-*b*]indole-2,10-diyl))bis(methanylylidene))bis(5,6-dichloro-3-oxo-2,3-dihydro-1*H*-indene-2,1-diylidene))dimalononitrile (BTP-4Cl or Y7). All materials were purchased from 1-materials or Sigma Aldrich.

Substrates were prepared from solution according the optimized recipe (18 mg/ml, 1:1.2 polymer:NFA, dissolved in CF with 1-chloronaphthalene 0.5 v/v%)^[33, 34], which was spin-coated with 3000 rpm for 30 s on substrates (10 mm x 10 mm for TA, 20 mm x 20 mm for PLDMR/trEPR) and annealed at 110°C for 10 min. TA samples were encapsulated under nitrogen atmosphere with 20 x 20 x 0.2 mm cover glass. Samples for PLDMR and trEPR were cut into strips of 2 mm width, whereby 10 strips were placed in an EPR quartz tube (Wilmad O.D. 4mm). The sample tubes were sealed under inert helium atmosphere. For EPR measurements on drop-cast samples, materials and blends were dissolved in chlorobenzene (5 mg/ml for PLDMR, 20 mg/ml for trEPR) and ~100 µl were poured into an EPR quartz tube. The solvent was then evaporated by vacuum pumping, creating a thin film on the EPR tube wall. The sample tubes were also sealed under inert helium atmosphere.

PLDMR and trEPR experiments were carried out with a modified X-band spectrometer (Bruker E300) equipped with a continuous-flow helium cryostat (Oxford ESR 900) and a microwave cavity (Bruker ER4104OR, 9.43 GHz) with optical access. All measurements were performed at $T = 10$ K.

For PLDMR, microwaves were generated with a microwave signal generator (Anritsu MG3694C), amplified to 3 W (microsemi) and guided into the cavity. Optical irradiation was performed with a 473 nm continuous wave laser (Cobolt). PL was detected with a silicon photodiode (Hamamatsu S2281) on the opposite opening of the cavity, using a 561 nm longpass filter to reject the excitation light. The PL signal was amplified by a current/voltage amplifier (Femto DHPVA-100) and recorded by lock-in detector (Ametek SR 7230), referenced by on-off-modulating the microwaves with 517 Hz.

For trEPR, pulsed optical excitation was performed with a Nd:YAG laser (Continuum Minilite II) with 532 nm; pulselength of 5 ns; 15 Hz repetition rate; 2 mJ per pulse. Microwaves were generated and detected with a microwave bridge (Bruker ER047MRP). Measurements were performed with 20 dB attenuation (2 mW). A voltage amplifier (FEMTO DHPVA-200) and a digitizer card (GaGe Razor Express 1642 CompuScope) were used for transient recording. The time resolution is limited to ~ 100 ns by the cavity Q factor of around 2800. By sweeping the magnetic field, two-dimensional data sets are recorded, where trEPR spectra are averaged from 0.5 – 1.5 μ s after laser excitation.

For TA, a setup powered by a Yb amplifier (PHAROS, Light Conversion), operating at 38 kHz and generating 200 fs pulses centred at 1030 nm with an output of 14.5 W, was used. The ~ 200 fs pump pulse was provided by an optical parametric amplifier (Light Conversion ORPHEUS). The probe was provided by a white light supercontinuum generated in a YAG crystal from a small amount of the 1030 nm fundamental. After passing through the sample, the probe is imaged using a Si photodiode array (Stresing S11490).

Quantum-chemical calculations were carried out to assess the singlet and triplet vertical excitation energies of three donor tetramers (PBDB-T, PM6 and PM7) and three NFAs (Y5, Y6, Y7) by using time-dependent DFT calculations within the Tamm-Dancoff approximation (TDA).^[61] For these calculations we employed an optimally-tuned *screened* range-separated hybrid (SRSH)^[60] LC- ω hPBE/6-311G(d,p) level of theory, where the scalar dielectric constant was set at 4.5. In addition, SOC matrix elements were computed in the Brett-Pauli spin-orbit Hamiltonian framework as implemented in the PySOC code^[75], performing the calculations at the ω B97X-D/Def2-TZVP level on the NFA Y-series S_1 optimized structure. All the calculations were carried out with the Gaussian16 suite^[76]. Further details can be found in SI.

Acknowledgements

J.G., V.D. and A.S. acknowledge support by the Deutsche Forschungsgemeinschaft (DFG, German Research Foundation) within the Research Training School “Molecular biradicals: Structure, properties and reactivity” (GRK2112). M.K., V.D. and A.S. acknowledge EU H2020 for funding through the Grant SEPOMO (Marie Skłodowska-Curie Grant Agreement 722651). Computational resources were provided by the Consortium des Équipements de Calcul Intensif (CÉCI), funded by the Fonds de la Recherche Scientifiques de Belgique (F.R.S.-FNRS) under Grant No. 2.5020.11, as well as the Tier-1 supercomputer of the Fédération Wallonie-Bruxelles, infrastructure funded by the Walloon Region under Grant Agreement No. 1117545. G.L. and Y.O. acknowledges funding by the Fonds de la Recherche Scientifique-FNRS under Grant No. F.4534.21 (MIS-IMAGINE). A.J.G acknowledges support from the EPSRC (EP/M01083X/1 and EP/M005143/1) and the Strategic University Network to Revolutionise Indian Solar Energy (SUNRISE), EPSRC Grant No. EP/P032591/1. The authors thank David Beljonne for fruitful discussion.

Data Availability

All data needed to evaluate the conclusions in the paper are present in the paper and/or the Supplementary Information.

Conflicts of interest

There are no conflicts to declare.

Authors contributions

J.G., B.S., and S.L. performed the magnetic resonance measurements and evaluated the data. G.L. and Y.O. performed the calculations. A.J.G. performed the transient absorption measurements. J.G. and A.S. wrote the manuscript, which all authors discussed and commented on.

Supplementary Materials

Supporting Information contains supplementary explanation and data, including additional TA spectra, computational details, additional PLDMR/trEPR spectra and triplet simulation parameters. SI includes Figures S1 – S18, Table S1 – S7.

ORCID

Jeannine Grüne: [0000-0003-3579-0455](https://orcid.org/0000-0003-3579-0455)

Giacomo Londi: [0000-0001-7777-9161](https://orcid.org/0000-0001-7777-9161)

Alexander J. Gillett: [0000-0001-7572-7333](https://orcid.org/0000-0001-7572-7333)

Yoann Olivier: [0000-0003-2193-1536](https://orcid.org/0000-0003-2193-1536)

Vladimir Dyakonov: [0000-0001-8725-9573](https://orcid.org/0000-0001-8725-9573)

Andreas Sperlich: [0000-0002-0850-6757](https://orcid.org/0000-0002-0850-6757)

References

- [1] Y. Lin, J. Wang, Z. G. Zhang, H. Bai, Y. Li, D. Zhu and X. Zhan, *Adv. Mater.* **2015**, 27, 1170-1174.
- [2] Y. Cui, Y. Xu, H. Yao, P. Bi, L. Hong, J. Zhang, Y. Zu, T. Zhang, J. Qin and J. Ren, *Adv. Mater.* **2021**, 33, 2102420.
- [3] A. J. Gillett, A. Privitera, R. Dilmurat, A. Karki, D. Qian, A. Pershin, G. Londi, W. K. Myers, J. Lee, J. Yuan, S.-J. Ko, M. Riede, F. Gao, G. Bazan, A. Rao, T.-Q. Nguyen, D. Beljonne and R. H. Friend, *Nature* **2021**, 597, 5.
- [4] Z. Chen, X. Chen, Z. Jia, G. Zhou, J. Xu, Y. Wu, X. Xia, X. Li, X. Zhang and C. Deng, *Joule* **2021**.
- [5] J. Hofinger, C. Putz, F. Mayr, K. Gugujonovic, D. Wielend and M. C. Scharber, *Mater. Adv.* **2021**.
- [6] V. C. Nikolis, J. Benduhn, F. Holzmueller, F. Piersimoni, M. Lau, O. Zeika, D. Neher, C. Koerner, D. Spoltore and K. Vandewal, *Adv. Energy Mater.* **2017**, 7, 1700855.
- [7] J. Benduhn, F. Piersimoni, G. Londi, A. Kirch, J. Widmer, C. Koerner, D. Beljonne, D. Neher, D. Spoltore and K. Vandewal, *Adv. Energy Mater.* **2018**, 8, 1800451.
- [8] W. Shockley and H. J. Queisser, *J. Appl. Phys.* **1961**, 32, 510-519.
- [9] U. Rau, *Phys. Rev. B* **2007**, 76, 085303.
- [10] X. Wan, C. Li, M. Zhang and Y. Chen, *Chem. Soc. Rev.* **2020**, 49, 2828-2842.
- [11] S. Karuthedath, J. Gorenflot, Y. Firdaus, N. Chaturvedi, C. S. De Castro, G. T. Harrison, J. I. Khan, A. Markina, A. H. Balawi and T. A. D. Peña, *Nat. Mater.* **2021**, 20, 378-384.
- [12] W. Chang, D. N. Congreve, E. Hontz, M. E. Bahlke, D. P. McMahon, S. Reineke, T. C. Wu, V. Bulović, T. Van Voorhis and M. A. Baldo, *Nat. Commun.* **2015**, 6, 1-6.
- [13] I. Ramirez, A. Privitera, S. Karuthedath, A. Jungbluth, J. Benduhn, A. Sperlich, D. Spoltore, K. Vandewal, F. Laquai and M. Riede, *Nat. Commun.* **2021**, 12, 1-10.
- [14] S. A. Thomson, J. Niklas, K. L. Mardis, C. Mallares, I. D. Samuel and O. G. Poluektov, *J. Phys. Chem. C* **2017**, 121, 22707-22719.
- [15] A. Rao, P. C. Chow, S. Gélinas, C. W. Schlenker, C.-Z. Li, H.-L. Yip, A. K.-Y. Jen, D. S. Ginger and R. H. Friend, *Nature* **2013**, 500, 435-439.
- [16] R. Wang, J. Yuan, R. Wang, G. Han, T. Huang, W. Huang, J. Xue, H. C. Wang, C. Zhang and C. Zhu, *Adv. Mater.* **2019**, 31, 1904215.
- [17] J. Han, X. Wang, D. Huang, C. Yang, R. Yang and X. Bao, *Macromolecules* **2020**, 53, 6619-6629.
- [18] L. Ma, H. Yao, J. Wang, Y. Xu, M. Gao, Y. Zu, Y. Cui, S. Zhang, L. Ye and J. Hou, *Angew. Chem.* **2021**.
- [19] Y. Xiang, Y. Zhao, N. Xu, S. Gong, F. Ni, K. Wu, J. Luo, G. Xie, Z.-H. Lu and C. Yang, *J. Mater. Chem. C* **2017**, 5, 12204-12210.
- [20] Q. Fan, U. A. Méndez-Romero, X. Guo, E. Wang, M. Zhang and Y. Li, *Chemistry—An Asian Journal* **2019**, 14, 3085-3095.
- [21] M. S. Kotova, G. Londi, J. Junker, S. Dietz, A. Privitera, K. Tvingstedt, D. Beljonne, A. Sperlich and V. Dyakonov, *Mater. Horiz.* **2020**, 7, 1641-1649.
- [22] J. Grüne, V. Dyakonov and A. Sperlich, *Mater. Horiz.* **2021**.
- [23] I. Sudakov, M. Van Landeghem, R. Lenaerts, W. Maes, S. Van Doorslaer and E. Goovaerts, *Adv. Energy Mater.* **2020**, 10, 2002095.
- [24] H. Kraus, M. C. Heiber, S. Vöth, J. Kern, C. Deibel, A. Sperlich and V. Dyakonov, *Sci. Rep.* **2016**, 6, 1-8.
- [25] A. Privitera, J. Grüne, A. Karki, W. K. Myers, V. Dyakonov, T. Q. Nguyen, M. K. Riede, R. H. Friend, A. Sperlich and A. J. Gillett, *Adv. Energy Mater.* **2022**, 2103944.
- [26] E. Goovaerts, *eMagRes* **2007**, 343-358.
- [27] S. Vöth, K. Tvingstedt, M. Auth, A. Sperlich, A. Dabuliene, J. V. Grazulevicius, P. Stakhira, V. Cherpak and V. Dyakonov, *Adv. Opt. Mater.* **2017**, 5, 1600926.

- [28] T. Biskup, *Front. Chem.* **2019**, 7, 10.
- [29] S. Weber, *eMagRes* **2007**, 255-270.
- [30] S. Richert, C. E. Tait and C. R. Timmel, *J. Magn. Reson.* **2017**, 280, 103-116.
- [31] G. Jeschke, *Macromol. Rapid Commun.* **2002**, 23, 227-246.
- [32] S. S. Eaton, K. M. More, B. M. Sawant and G. R. Eaton, *Journal of the American Chemical Society* **1983**, 105, 6560-6567.
- [33] R. Ma, T. Yang, Y. Xiao, T. Liu, G. Zhang, Z. Luo, G. Li, X. Lu, H. Yan and B. Tang, *Energy Environ. Mater.* **2021**.
- [34] F. D. Eisner, M. Azzouzi, Z. Fei, X. Hou, T. D. Anthopoulos, T. J. S. Dennis, M. Heeney and J. Nelson, *Journal of the American Chemical Society* **2019**, 141, 6362-6374.
- [35] S. Stoll and A. Schweiger, *J. Magn. Reson.* **2006**, 178, 42-55.
- [36] J. De Ceuster, E. Goovaerts, A. Bouwen and V. Dyakonov, *Phys. Rev. B* **2003**, 68, 125202.
- [37] J. Shinar, *Laser & Photonics Reviews* **2012**, 6, 767-786.
- [38] B. Z. Tedlla, F. Zhu, M. Cox, B. Koopmans and E. Goovaerts, *Phys. Rev. B* **2015**, 91, 085309.
- [39] T. Biskup, M. Sommer, S. Rein, D. L. Meyer, M. Kohlstädt, U. Würfel and S. Weber, *Angew. Chem. Int. Ed.* **2015**, 54, 7707-7710.
- [40] L. Zhu, M. Zhang, G. Zhou, T. Hao, J. Xu, J. Wang, C. Qiu, N. Prine, J. Ali and W. Feng, *Adv. Energy Mater.* **2020**, 10, 1904234.
- [41] G. Zhang, X.-K. Chen, J. Xiao, P. C. Chow, M. Ren, G. Kupgan, X. Jiao, C. Chan, X. Du and R. Xia, *Nat. Commun.* **2020**, 11, 1-10.
- [42] Y. Li, H. Meng, J. Huang and C. Zhan, *ACS Appl. Mater. Interfaces* **2020**, 12, 50541-50549.
- [43] J. Yuan, Y. Zhang, L. Zhou, G. Zhang, H.-L. Yip, T.-K. Lau, X. Lu, C. Zhu, H. Peng and P. A. Johnson, *Joule* **2019**, 3, 1140-1151.
- [44] A. Karki, J. Vollbrecht, A. L. Dixon, N. Schopp, M. Schrock, G. M. Reddy and T. Q. Nguyen, *Adv. Mater.* **2019**, 31, 1903868.
- [45] V. Vohra, K. Kawashima, T. Kakara, T. Koganezawa, I. Osaka, K. Takimiya and H. Murata, *Nat. Photonics* **2015**, 9, 403-408.
- [46] C. Grieco, G. S. Doucette, R. D. Pensack, M. M. Payne, A. Rimshaw, G. D. Scholes, J. E. Anthony and J. B. Asbury, *Journal of the American Chemical Society* **2016**, 138, 16069-16080.
- [47] Y. Zhang and S. R. Forrest, *Chem. Phys. Lett.* **2013**, 590, 106-110.
- [48] E. Hontz, W. Chang, D. N. Congreve, V. Bulović, M. A. Baldo and T. Van Voorhis, *J. Phys. Chem. C* **2015**, 119, 25591-25597.
- [49] A. J. Gillett, C. Tonnelé, G. Londi, G. Ricci, M. Catherin, D. M. Unson, D. Casanova, F. Castet, Y. Olivier and W. M. Chen, *Nat. Commun.* **2021**, 12, 1-10.
- [50] D. Beljonne, Z. Shuai, G. Pourtois and J. Bredas, *J. Phys. Chem. A* **2001**, 105, 3899-3907.
- [51] E. W. Evans, Y. Olivier, Y. Puttisong, W. K. Myers, T. J. Hele, S. M. Menke, T. H. Thomas, D. Credginton, D. Beljonne and R. H. Friend, *J. Phys. Chem. Lett.* **2018**, 9, 4053-4058.
- [52] A. Karki, J. Vollbrecht, A. J. Gillett, S. S. Xiao, Y. Yang, Z. Peng, N. Schopp, A. L. Dixon, S. Yoon and M. Schrock, *Energy Environ. Sci.* **2020**, 13, 3679-3692.
- [53] R. Wang, C. Zhang, Q. Li, Z. Zhang, X. Wang and M. Xiao, *Journal of the American Chemical Society* **2020**, 142, 12751-12759.
- [54] L. Qin, X. Liu, X. Zhang, J. Yu, L. Yang, F. Zhao, M. Huang, K. Wang, X. Wu and Y. Li, *Angew. Chem. Int. Ed.* **2020**, 59, 15043-15049.
- [55] R. Ma, T. Liu, Z. Luo, Q. Guo, Y. Xiao, Y. Chen, X. Li, S. Luo, X. Lu and M. Zhang, *Sci. China: Chem* **2020**, 63, 325-330.
- [56] Y. Zhong, M. Causa, G. J. Moore, P. Krauspe, B. Xiao, F. Günther, J. Kublitski, R. Shivhare, J. Benduhn and E. BarOr, *Nat. Commun.* **2020**, 11, 1-10.
- [57] S. Natsuda, T. Saito, R. Shirouchi, Y. Sakamoto, T. Takeyama, Y. Tamai and H. Ohkita, *Energy Environ. Sci.* **2022**, 15, 1545-1555.
- [58] F. Liu, L. Zhou, W. Liu, Z. Zhou, Q. Yue, W. Zheng, R. Sun, W. Liu, S. Xu and H. Fan, *Adv. Mater.* **2021**, 33, 2100830.
- [59] J. Wu, J. Lee, Y.-C. Chin, H. Yao, H. Cha, J. Luke, J. Hou, J.-S. Kim and J. R. Durrant, *Energy Environ. Sci.* **2020**, 13, 2422-2430.

- [60] S. Refaely-Abramson, S. Sharifzadeh, N. Govind, J. Autschbach, J. B. Neaton, R. Baer and L. Kronik, *Phys. Rev. Lett.* **2012**, 109, 226405.
- [61] S. Hirata and M. Head-Gordon, *Chem. Phys. Lett.* **1999**, 314, 291-299.
- [62] S. Lower and M. El-Sayed, *Chem. Rev.* **1966**, 66, 199-241.
- [63] M. A. El-Sayed, *Acc. Chem. Res.* **1968**, 1, 8-16.
- [64] G. Han, T. Hu and Y. Yi, *Adv. Mater.* **2020**, 32, 2000975.
- [65] C. Ma, C. C. Chan, X. Zou, H. Yu, J. Zhang, H. Yan, K. S. Wong and P. C. Chow, *Solar RRL* **2021**, 5, 2000789.
- [66] S. M. Menke, A. Sadhanala, M. Nikolka, N. A. Ran, M. K. Ravva, S. Abdel-Azeim, H. L. Stern, M. Wang, H. Sirringhaus and T.-Q. Nguyen, *ACS nano* **2016**, 10, 10736-10744.
- [67] J. Wang, X. Gu, H. Ma, Q. Peng, X. Huang, X. Zheng, S. H. Sung, G. Shan, J. W. Lam and Z. Shuai, *Nat. Commun.* **2018**, 9, 1-9.
- [68] Q. Fan, T. Liu, W. Gao, Y. Xiao, J. Wu, W. Su, X. Guo, X. Lu, C. Yang and H. Yan, *J. Mater. Chem. A* **2019**, 7, 15404-15410.
- [69] R. Ma, G. Li, D. Li, T. Liu, Z. Luo, G. Zhang, M. Zhang, Z. Wang, S. Luo and T. Yang, *Solar RRL* **2020**, 4, 2000250.
- [70] N. D. Eastham, J. L. Logsdon, E. F. Manley, T. J. Aldrich, M. J. Leonardi, G. Wang, N. E. Powers-Riggs, R. M. Young, L. X. Chen and M. R. Wasielewski, *Adv. Mater.* **2018**, 30, 1704263.
- [71] Y. Cui, H. Yao, J. Zhang, T. Zhang, Y. Wang, L. Hong, K. Xian, B. Xu, S. Zhang and J. Peng, *Nat. Commun.* **2019**, 10, 1-8.
- [72] Q. Fan, Q. Zhu, Z. Xu, W. Su, J. Chen, J. Wu, X. Guo, W. Ma, M. Zhang and Y. Li, *Nano Energy* **2018**, 48, 413-420.
- [73] Z. Liu, Y. Gao, J. Dong, M. Yang, M. Liu, Y. Zhang, J. Wen, H. Ma, X. Gao and W. Chen, *J. Phys. Chem. Lett.* **2018**, 9, 6955-6962.
- [74] G. Dennler, M. C. Scharber and C. J. Brabec, *Adv. Mater.* **2009**, 21, 1323-1338.
- [75] X. Gao, S. Bai, D. Fazzi, T. Niehaus, M. Barbatti and W. Thiel, *J. Chem. Theory Comput.* **2017**, 13, 515-524.
- [76] M. J. Frisch, G. W. Trucks, H. B. Schlegel, G. E. Scuseria, M. A. Robb, J. R. Cheeseman, G. Scalmani, V. Barone, G. A. Petersson, H. Nakatsuji, X. Li, M. Caricato, A. V. Marenich, J. Bloino, B. G. Janesko, R. Gomperts, B. Mennucci, H. P. Hratchian, J. V. Ortiz, A. F. Izmaylov, J. L. Sonnenberg, Williams, F. Ding, F. Lipparini, F. Egidi, J. Goings, B. Peng, A. Petrone, T. Henderson, D. Ranasinghe, V. G. Zakrzewski, J. Gao, N. Rega, G. Zheng, W. Liang, M. Hada, M. Ehara, K. Toyota, R. Fukuda, J. Hasegawa, M. Ishida, T. Nakajima, Y. Honda, O. Kitao, H. Nakai, T. Vreven, K. Throssell, J. A. Montgomery Jr., J. E. Peralta, F. Ogliaro, M. J. Bearpark, J. J. Heyd, E. N. Brothers, K. N. Kudin, V. N. Staroverov, T. A. Keith, R. Kobayashi, J. Normand, K. Raghavachari, A. P. Rendell, J. C. Burant, S. S. Iyengar, J. Tomasi, M. Cossi, J. M. Millam, M. Klene, C. Adamo, R. Cammi, J. W. Ochterski, R. L. Martin, K. Morokuma, O. Farkas, J. B. Foresman and D. J. Fox, Gaussian, Inc., Wallingford CT, 2016.

SUPPORTING INFORMATION

for

Energetically Trapped Triplet Excitons and their Generation Pathways in Organic Solar Cell Blends based on (Non-) Halogenated PBDB-T and Y-Series

Jeannine Grüne^{1*}, Giacomo Londi², Alexander J. Gillett³, Basil Stähly¹, Sebastian Lulei¹, Maria Kotova¹, Yoann Olivier², Vladimir Dyakonov¹, and Andreas Sperlich^{1*}

¹Experimental Physics 6, Julius Maximilian University of Würzburg, Am Hubland, 97074 Würzburg, Germany

²Laboratory for Computational Modeling of Functional Materials, Namur Institute of Structured Matter, University of Namur, Rue de Bruxelles, 61, 5000 Namur, Belgium

³Cavendish Laboratory, University of Cambridge, JJ Thomson Avenue, Cambridge, UK

* jeannine.gruene@physik.uni-wuerzburg.de, sperlich@physik.uni-wuerzburg.de

Contents

| | |
|--|----|
| 1. Energy Levels..... | 23 |
| 2. Additional trEPR and TA Data for Y6 Blended Spin-Coated Substrates..... | 23 |
| TA Measurements | 23 |
| trEPR Measurements..... | 24 |
| 3. Transient Absorption Measurements on NFA Y7..... | 25 |
| Halogenation of the Donor..... | 25 |
| Influence of the Solvent | 26 |
| 4. Computational Details..... | 27 |
| 5. Additional PLDMR Data | 30 |
| 6. trEPR Signal Pattern and Additional Data..... | 32 |
| trEPR Pattern by SOC-Driven ISC..... | 32 |
| trEPR Pattern by Geminate Back Charge Transfer | 33 |
| Additional trEPR Spectra | 34 |
| 7. HOMO/LUMO Level..... | 35 |
| 8. Triplet Simulation Parameters..... | 36 |
| PLDMR | 36 |
| trEPR..... | 38 |

1. Energy Levels

| Material | S_1 [eV] | ΔE_{ST} [eV] | T_1, T_2 [eV] | CT [eV] | Triplets | Mechanism | Refs. for S_1, CT |
|-----------|------------|----------------------|-----------------|---------|----------|---------------|---------------------|
| PBDB-T | 1.85 | 0.40 | 1.45 | | | ISC | [1, 2] |
| PM6 | 1.92 | 0.41 | 1.51 | | | ISC | [3, 4] |
| PM7 | 1.92 | 0.41 | 1.51 | | | ISC | [5] |
| Y6 | 1.39 | 0.56, 0.35 | 0.83, 1.04 | | | ISC | [2, 3, 6-10] |
| Y7 | 1.40 | 0.55, 0.34 | 0.85, 1.06 | | | ISC | [11] |
| PBDB-T:Y6 | | | | 1.35 | Y6 | HBT (ng) | [12] |
| PM6:Y6 | | | | 1.37 | Y6 | ISC, HBT (ng) | [2, 7, 10, 13, 14] |
| PM7:Y6 | | | | 1.37 | Y6 | ISC, HBT (ng) | [15] |
| PBDB-T:Y7 | | | | 1.36 | Y7 | HBT (ng) | [15] |
| PM6:Y7 | | | | 1.38 | Y7 | ISC, HBT (ng) | [12] |
| PM7:Y7 | | | | 1.38 | Y7 | ISC, HBT (ng) | n.a. |

Table S1. Energy values for donor polymers PBDB-T, PM6, PM7 and acceptors Y6, Y7. S_1 and CT energies of experimentally determined values are taken from given references (averaged values). Triplet energies are determined by subtraction of calculated ΔE_{ST} from S_1 . CT singlet and triplet energies are treated as isoenergetic. Triplets in blends are localized on acceptor molecules populated by different formation mechanisms (ng = non-geminate). The CT value for PM7:Y7 is assumed to be identical with PM6:Y6 because PM6 and PM7 have identical energy levels.

2. Additional trEPR and TA Data for Y6 Blended Spin-Coated Substrates

The optimized recipe for PM6:Y6 solar cells have a spin-coated active layer of 14 – 18 mg/ml PM6:Y6 blend in a ratio of 1:1.2 dissolved in CF with 0.5% v/v 1-chloronaphthalene.^[16, 17] The solution is spin-coated with 3000 rpm for 30 sec and subsequently annealed at 110° for 10 min. The blends for the other donor:acceptor combinations are prepared with the same recipe. While TA measurements are performed on glass substrates with size of 10x10 mm (encapsulated with 20x20 mm cover slip of 0.2 mm thickness), for EPR measurements, 20x20 mm cover slips were cut into strips of 2 mm width whereby 10 strips were placed into an EPR tube.

TA Measurements

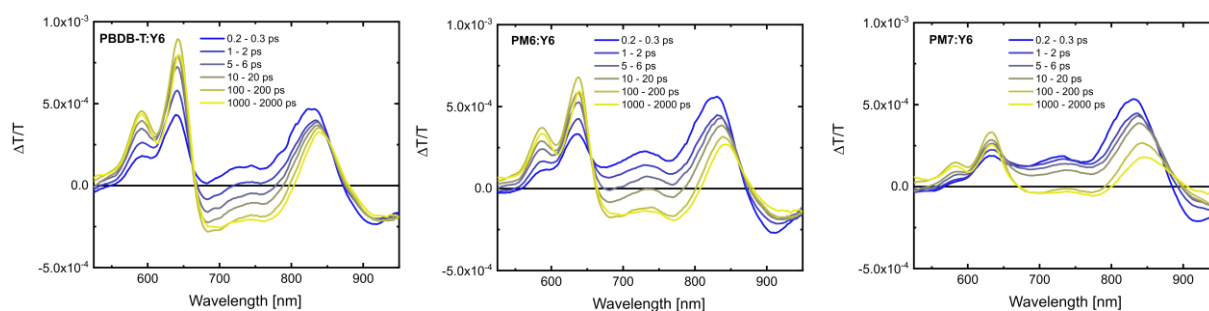


Figure S1 Transient absorption (TA) spectra of PBDB-T:Y6, PM6:Y6 and PM7:Y6. Excitation at 800 nm; fluence of $\sim 0.6 \mu\text{J cm}^{-2}$.

Figure S1 shows the TA measurements for PBDB-T:Y6, PM6:Y6 and PM7:Y6. All samples show a comparable Y6 GSB at 840 nm, indicating a comparable number of excitations created on Y6. While a clear polymer GSB is visible in PBDB-T:Y6 and PM6:Y6 already after 0.2 ps, the polymer GSB at 0.2 ps PM7:Y6 is very weakly pronounced. Comparing the intensity of polymer GSB when HT is completed at around 100 ps, the HT yield in PBDB-T:Y6 is the highest, followed by PM6:Y6 and PM7:Y6. In the same trend, the Y6 GSB is decaying slowest in PBDB-T:Y6, followed by PM6:Y6 and PM7:Y6. While the HT kinetics are comparable in all three blends, the faster Y6 GSB decay is most likely due to undissociated Y6 S_1 excitons recombining to the ground state or undergoing ISC.

trEPR Measurements

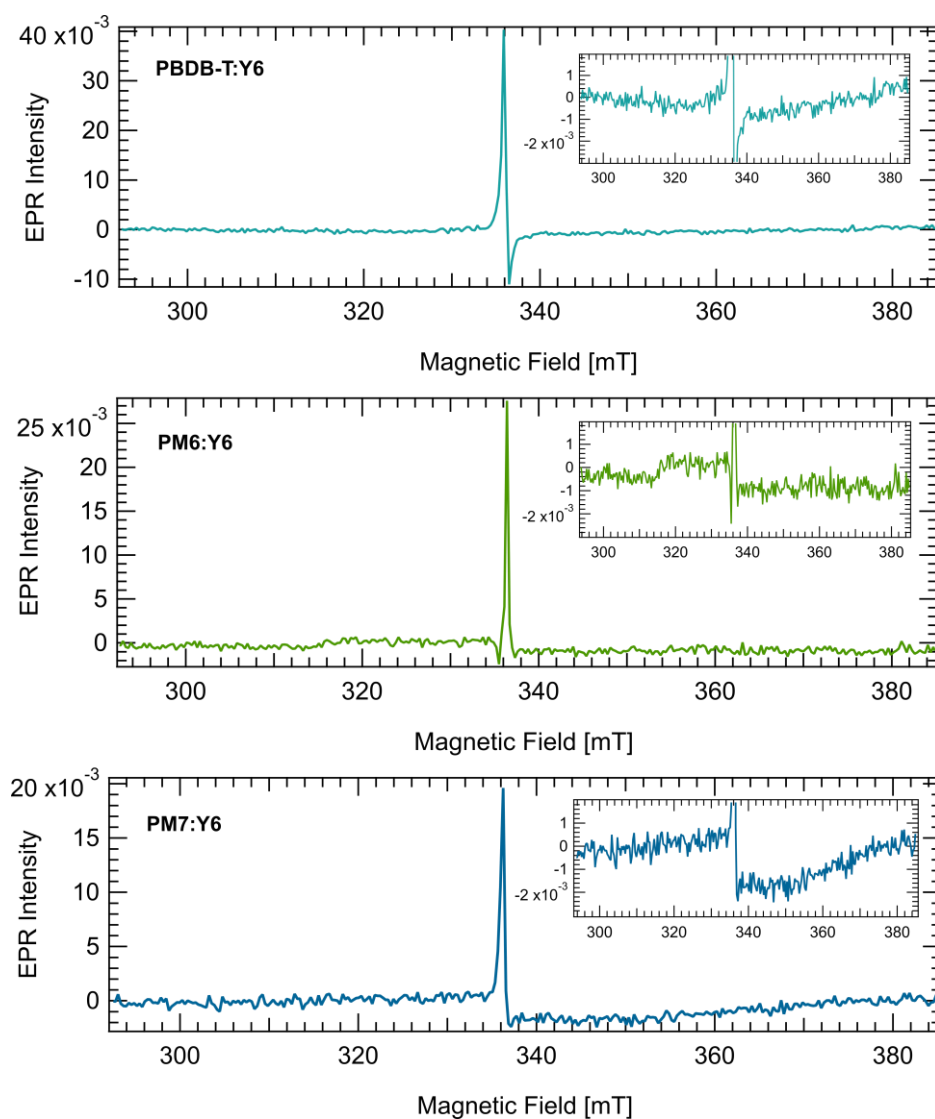


Figure S2. trEPR measurements on spin-coated substrates for Y6 blends. All blends possess an intense CT peak whereby PM6:Y6 and PM7:Y6 show a small ISC yield.

Figure S2 shows the trEPR measurements on spin-coated substrates for Y6 blends. As for the dropcast samples in Figure 2, an ISC yield is visible for PM6:Y6 and PM7:Y6, as already shown in literature for spin-coated PM6:Y6 substrates.^[14] In contrast to the dropcast samples of Figure 2, the molecular triplet signal is smaller. On the one hand, the smaller amount of materials on the substrates and, on the other hand, the increased HT yield in spin-coated films reduces the molecular signal. The exact pattern cannot be determined from this signal-to-noise ratio, but it fits the emission/absorption in SOC-driven ISC as already observed in the dropcast samples. Moreover, the width corresponds to triplet excitons on the NFA. PBDB-T:Y6 shows the same trend in ISC yield as the dropcast samples with negligible trEPR signal, which is consistent with the HT measurements. Nevertheless, the ISC yield in the other two blends is also very low, so the competing process to HT from Figure S1 is most probably the S_1 decay to the ground state. Moreover, PBDB-T:Y6 shows the highest CT peak, indicating the highest fraction of CT states, while the CT peak decreases in PM7:Y6.

3. Transient Absorption Measurements on NFA Y7

Halogenation of the Donor

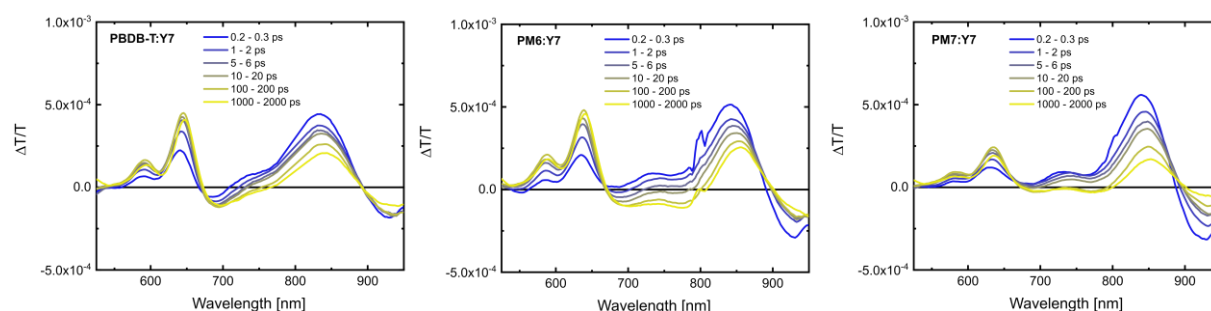


Figure S3. TA spectra for PBDB-T:Y7, PM6:Y7 and PM7:Y7. Excitation at 800 nm; fluence of $\sim 0.6 \mu\text{J cm}^{-2}$.

Figure S4 shows TA measurements for PBDB-T:Y7, PM6:Y7, and PM7:Y7. All samples show comparable Y7 GSB at 840 nm, indicating a comparable number of excitations generated on Y7. While the polymer GSB in PBDB-T:Y7 and PM6:Y7 is visible after 0.2 ps, the polymer GSB in PM7:Y7 is very weak. Comparing the intensities of the polymer GSB when the HT is completed at about 100 ps, the HT yield in PBDB-T:Y7 and PM6:Y7 is comparable, with PM7:Y7 exhibiting the lowest yield. PM7:Y7 also reveals the fastest decay of Y7 GSB, indicating the highest amount of undissociated S_1 excitons decaying to the ground state. Overall, the HT yield of Y7 blends is lower than that of Y6 blends, which may be due to the fact that CF is not the optimal solvent, as will be discussed in the next section. Comparing the HT kinetics of the polymer GSB between 580 and 650 nm of all blends with NFA Y7 together with the kinetics of Y6 blends (Figure S5), the HT kinetics for all six blends are comparable.

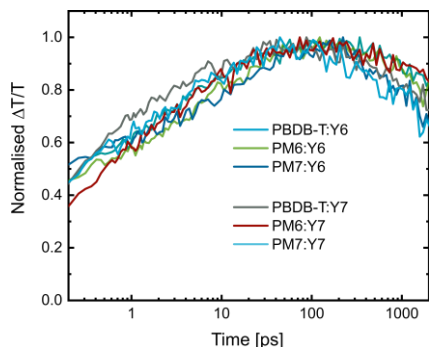


Figure S4. HT kinetics for all PM:Y series blends. HT rates extracted from polymer GSB 580 – 650 nm. All blends show comparable HT kinetics.

Influence of the Solvent

The stacking and crystallinity of the NFAs Y6 and Y7 strongly depends on the solvent. Y6 shows a more dominant crystalline orientation and a better π - π stacking in CF than in CB.^[18] However, the chlorination in NFA Y7 gives the molecule stronger tendency to aggregate thereafter a solvent with a higher boiling point as CB is suitable.^[19] The optimized recipe for PM6:Y7 solar cells are thus rather obtained with CB than CF as solvent.^[11, 19]

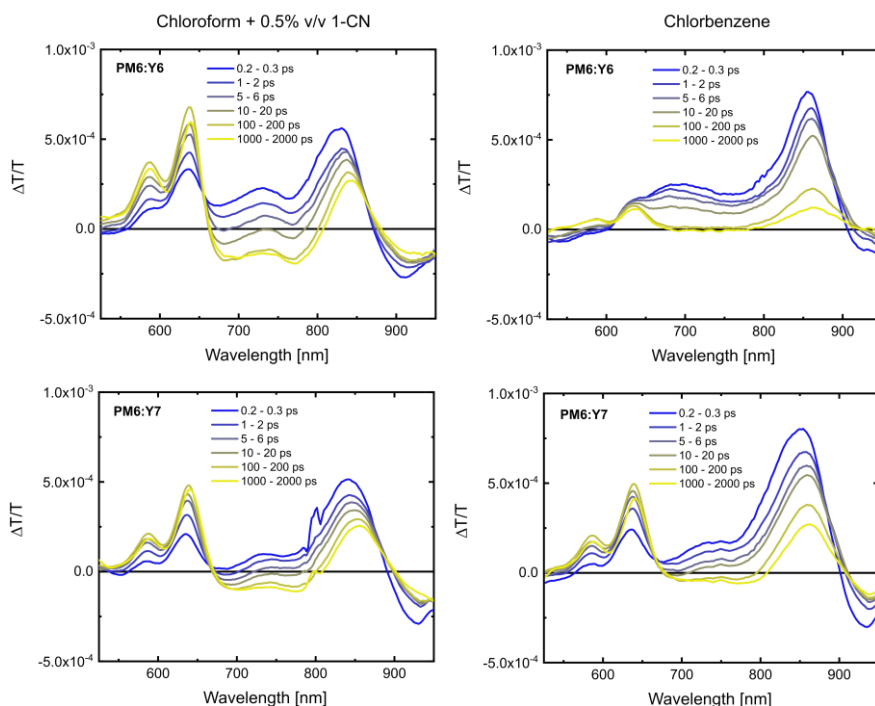


Figure S5. TA measurements for PM6:Y6 (top) and PM6:Y7 (bottom) dissolved in CF/1-CN (left) and CB (right). While the HT yield decreases in PM6:Y6 when changing CF with CB, the HT yield is comparable in PM6:Y7. Excitation at 800 nm; fluence of $\sim 0.6 \mu\text{J cm}^{-2}$.

Figure S5 shows TA measurements for PM6:Y6 (top) and PM6:Y7 (bottom) dissolved in CF/ 1-CN (left) and CB (right). While PM6:Y6 in CF shows a PM6 GSB already at 0.2 ps, significantly increasing up to

100 ps, PM6:Y6 in CB shows a considerable smaller PM6 GSB, first arising after 10 ps and not increasing in time. While the Y6 GSB is initially comparable, it decreases quickly in PM6:Y6 dissolved in CB, indicating a high amount of undissociated excitons. While the HT yield in PM6:Y6 significantly decreasing when going from CF to CB, the HT yield in PM6:Y7 is approximately comparable. These results agree with a reduced short-circuit current density j_{sc} in PM6:Y6 and enhanced j_{sc} in PM6:Y7 upon fabrication with CB instead of CF.^[18, 19] Thus, when using the optimized recipe for Y7 blends (in Figure S6 without 1-CN), Y7 blends could turn out to be better with this fabrication method as shown for the solar cells.

4. Computational Details

The gas-phase ground state equilibrium geometry of three donor tetramers (PBDB-T, PM6 and PM7) and three NFAs (Y5, Y6, Y7) was optimized at the DFT level, using the exchange-correlation functional ω B97X-D and the basis set 6-31G(d,p). In order to speed up the calculations, the alkyl chains were replaced with methyl groups, both in donors and NFA Y-series.^[20] Then, singlet and triplet vertical excitation energies were then assessed by means of time-dependent DFT calculations within the Tamm-Dancoff approximation (TDA).^[21] For such TDA TDDFT calculations, we resorted to a *screened* range-separated hybrid (SRSH) LC- ω hPBE functional and the 6-311G(d,p) basis set, as previously done elsewhere.^[14] In the SRSH approach, solid-state screening effects are introduced by adjusting two parameters, α and β in addition to the non-empirical tuning of the exchange range-separation parameter ω .^[22] The optimal gas-phase ω value was found following the gap-tuning procedure.^[23] Then, the dielectric constant of the surrounding medium was chosen at $\epsilon = 4.5$, α was fixed at 0.2, and, according to the relationship $\alpha + \beta = \frac{1}{\epsilon}$, β was set at 0.0222. All quantum-chemical calculations were carried out with the Gaussian16 suite.^[24]

| Material | f (osc. str.) | S_1 [eV] | T_1, T_2 [eV] | ΔE_{ST} [eV] |
|----------|-----------------|------------|-----------------|----------------------|
| PBDB-T | 5.031 | 2.21 | 1.81 | 0.40 |
| PM6 | 5.304 | 2.24 | 1.83 | 0.41 |
| PM7 | 5.398 | 2.24 | 1.83 | 0.41 |
| Y5 | 2.481 | 2.02 | 1.46 | 0.56 |
| Y6 | 2.461 | 2.00 | 1.44, 1.65 | 0.56, 0.35 |
| Y7 | 2.505 | 1.97 | 1.42, 1.63 | 0.55, 0.34 |

Table S2. Calculated singlet and triplet vertical excitation energies, including the oscillator strength f for singlet transitions. The computed ΔE_{ST} gap was then subtracted from experimental singlet energy values to accurately estimate T_1 and T_2 energies, as reported in Table S1.

The parameters that enter the Marcus-Levich-Jortner equation (see main text) were computed as follows. As regards the internal reorganization energy λ_i , we used the 4-points method, having performed gas-phase excited-state optimizations of S_1 and T_1 of the NFA Y-series at TDA TDDFT level, by employing the ω B97X-D functional and the 6-31G(d,p) basis set. Then, the energy differences

$\Delta E_{S_1-T_x}^0$ (where $x = 1$ and 2) were evaluated at the SRSH TDA TDDFT LC- ω hPBE/6-311G(d,p) level of theory on the excited-state optimized structures (eventually, we also optimized the T_2 state for this purpose). SOC matrix elements were computed in the Breit-Pauli spin-orbit Hamiltonian framework as implemented in the PySOC code.^[25] These calculations, on the other hand, were performed with the ω B97X-D functional and expanding the basis set to a Def2-TZVP, taking as input geometry the NFA Y-series S_1 optimized structure.

| NFA | $\Delta E_{S_1-T_1}^0$ [eV] | $\langle S_1 H_{SOC} T_1 \rangle$ [eV] | $\Delta E_{S_1-T_2}^0$ [eV] | $\langle S_1 H_{SOC} T_2 \rangle$ [eV] | λ_i [eV] |
|-----|-----------------------------|---|-----------------------------|---|------------------|
| Y5 | 0.59 | 7×10^{-6} | 0.36 | 1×10^{-5} | 0.040 |
| Y6 | 0.58 | 6×10^{-6} | 0.35 | 1×10^{-5} | 0.034 |
| Y7 | 0.57 | 6×10^{-6} | 0.34 | 1×10^{-5} | 0.032 |

Table S3. Calculated adiabatic energy differences between S_1 and the first two low-lying triplet states (T_1 and T_2), along with their corresponding SOC: $V_{SOC} = \langle S_1 | H_{SOC} | T_x \rangle$. The internal reorganization energy λ_i is also reported.

| λ_s [eV] | 0.05 | 0.10 | 0.15 | 0.20 | |
|---------------------|--------------------------------------|-----------------|-----------------|-----------------|-----------------|
| Material | κ_{ISC} [s ⁻¹] | | | | |
| Y5 | 2×10^5 | 5×10^5 | 1×10^6 | 2×10^6 | 7×10^4 |
| Y6 | 2×10^5 | 5×10^5 | 1×10^6 | 2×10^6 | 4×10^4 |
| Y7 | 2×10^5 | 5×10^5 | 1×10^6 | 2×10^6 | 4×10^4 |

Table S4. Computed ISC rates from S_1 to T_2 as a function of the external reorganization energy λ_s . For the sake of completeness, we also report in red the ISC rates from S_1 to T_1 , computed with $\lambda_s = 0.2$ eV.

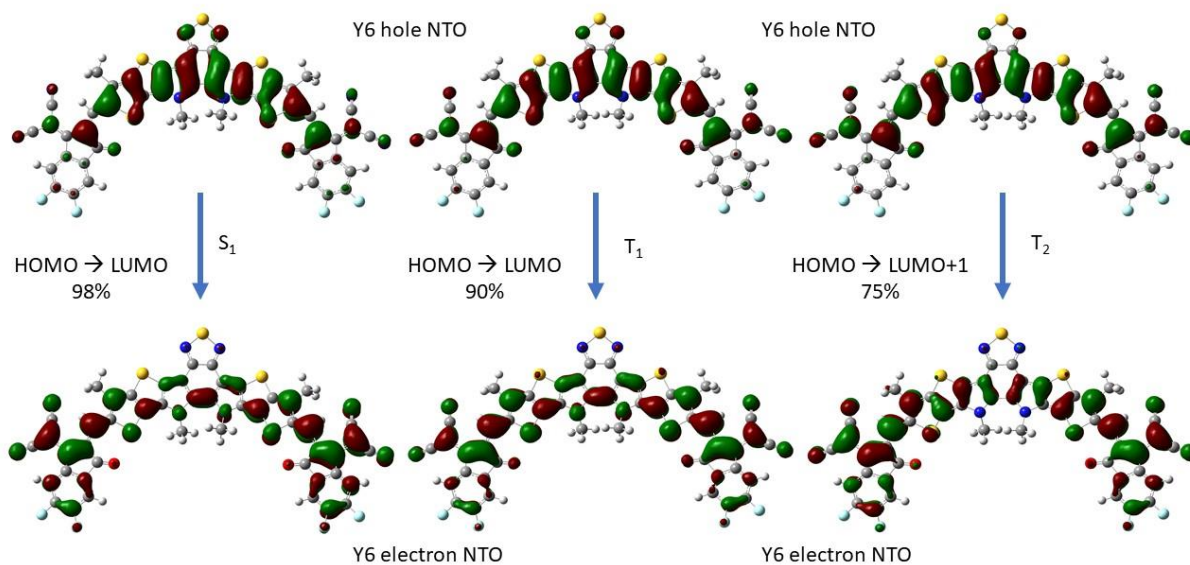


Figure S6. Hole and electron natural transition orbitals (NTOs) of Y6 as obtained at the SRSH TDA TDDFT LC- ω hPBE/6-311G(d,p) level of theory. The same NTOs were found for Y7, meaning that halogenation does not alter the nature of the low-lying excited states, namely S_1 and T_2 from which ISC can occur.

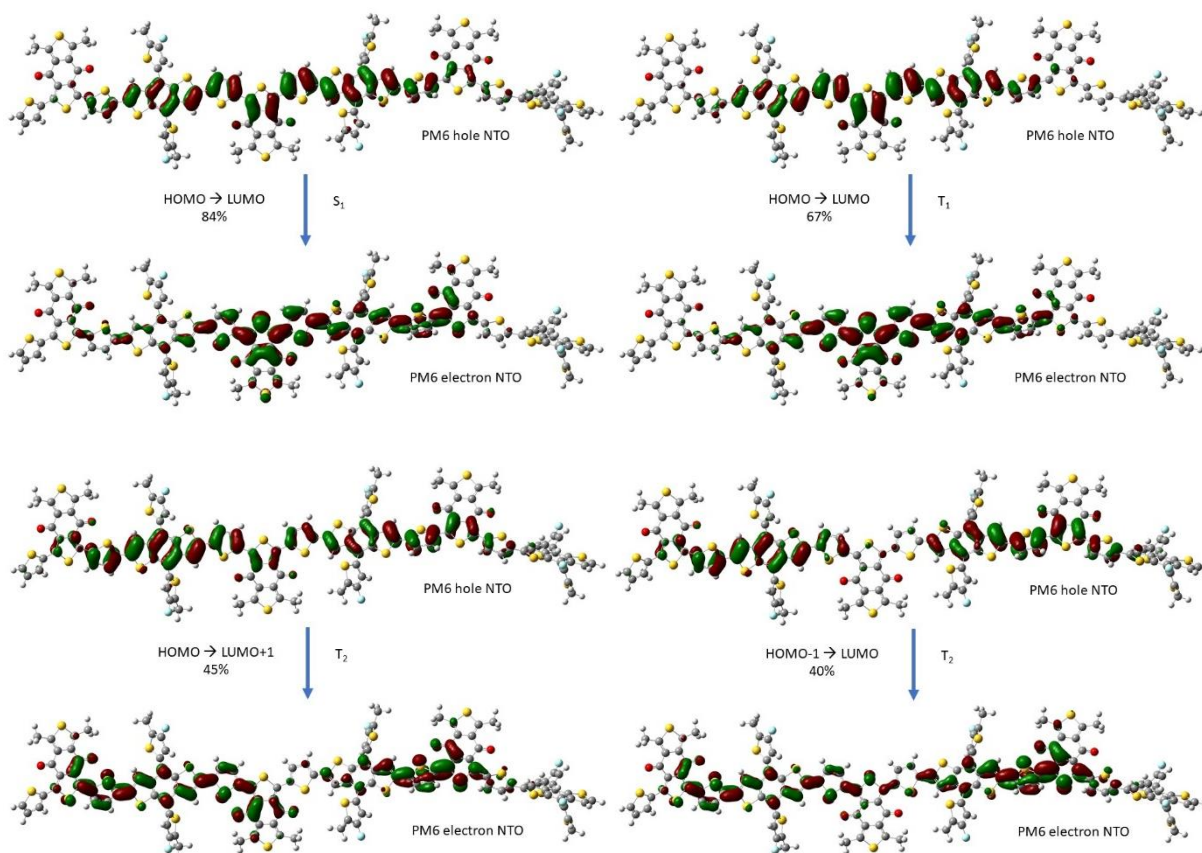


Figure S7. Hole and electron natural transition orbitals (NTOs) of a PM6 polymer chain as obtained at the SRSH TDA TDDFT LC- ω hPBE/6-311G(d,p) level of theory.

5. Additional PLDMR Data

The following part shows all PLDMR spectra of all polymers on spin-coated substrates (Figure S8) and PLDMR of dropcast samples of Y6 (Figure S9) and Y7 (Figure S10). The same presence of NFA triplet excitons can be found, whereby the width of the spectra are almost identical for dropcast and spin-coated samples. Only the ordering factor is higher for spin-coated substrates, as the molecules show preferential orientation on the substrate (Table S5 and S6). NFAs thereby stack face-on on the substrate, while the donors show a coexistence of edge-on and face-on orientation, which is visible by the shoulder in the HF signal and the additional smaller wings at 315 and 360 mT (Figure S8).^[18, 26, 27] In the blends, the face-on stacking of NFA remains.^[28]

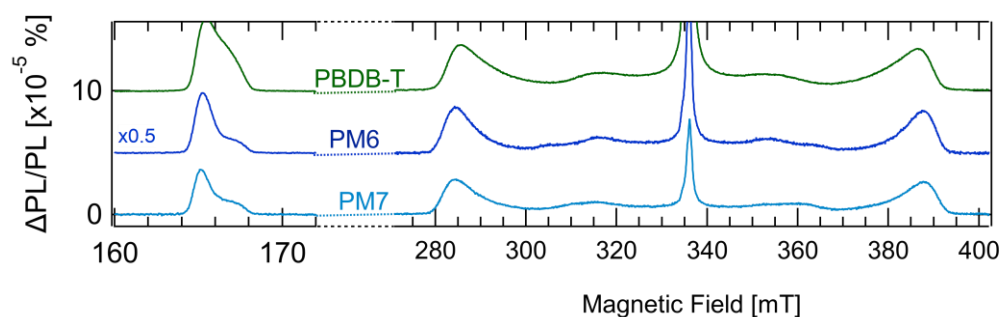


Figure S8. PLDMR spectra of the neat PBDB-T, PM6, PM7 on spin-coated substrates. The position of the HF signal and the width of the FF signal are similar (ZFS parameter in Table S5). Additionally, all PLDMR spectra show a considerable ordering (Table S5)

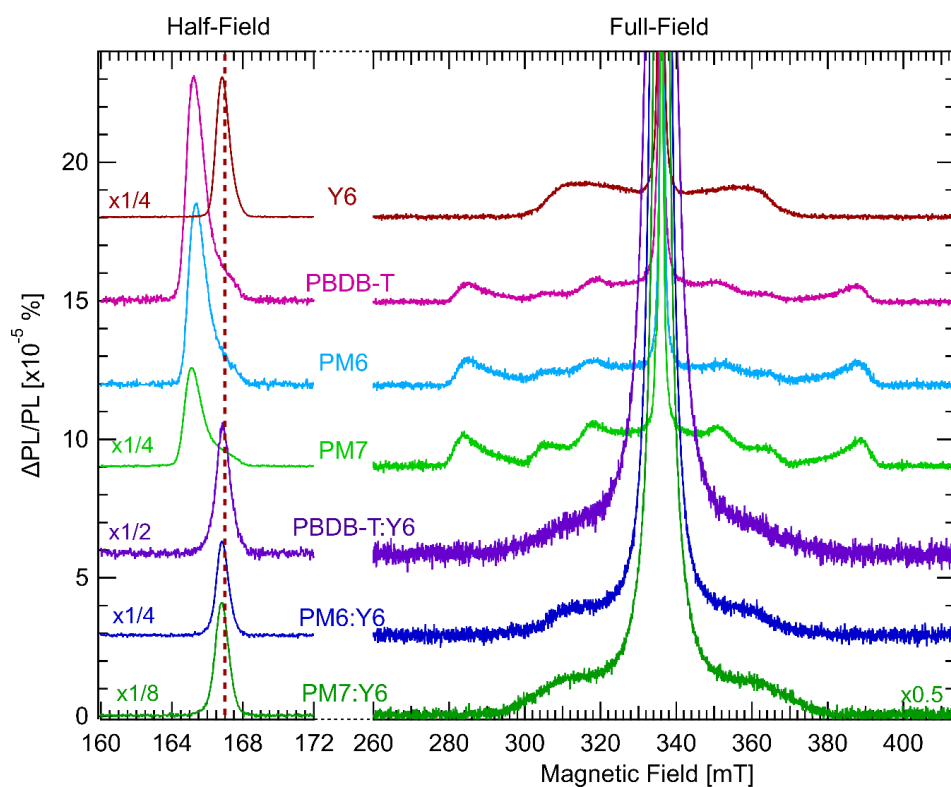


Figure S9. PLDMR spectra of the neat materials Y6, PBDB-T, PM6, PM7 and their blends PBDB-T:Y6, PM6:Y6 and PM7:Y6. The position of the HF signal and the width of the FF signal reveal Y6 triplet excitons in all blends.

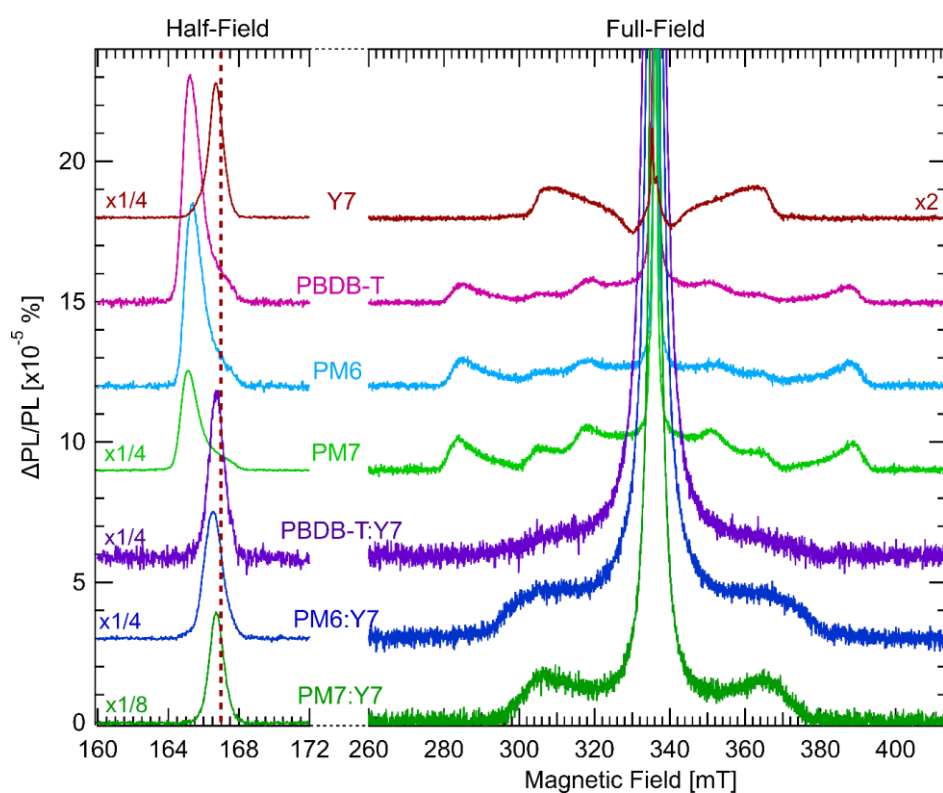


Figure S10. PLDMR spectra of neat materials Y7, PBDB-T, PM6, PM7 and their blends PBDB-T:Y7, PM6:Y7 and PM7:Y7. The position of the HF signal and the width of the FF signal reveal Y7 triplet excitons in all blends.

6. trEPR Signal Pattern and Additional Data

trEPR Pattern by SOC-Driven ISC

Spin-orbit coupling (SOC) is the dominant mechanism for ISC in small molecules since it decays rapidly with electron-hole distance with typical coupling values of few meV. At larger electron-hole distances, ISC is driven by the electron-hole distance-independent hyperfine interaction (HFI) which is typically negligible compared to SOC in small molecules.^[29] The trEPR pattern arising is drawn in Figure S3 for Y6 with zero-field populations $[p_z, p_y, p_x] = [0, 0.66, 0.34]$. SOC-driven ISC acts on the zero-field triplet states, given by the eigenstates of the Hamiltonian $|X\rangle$, $|Y\rangle$ and $|Z\rangle$, whose populations can be transferred to the populations of the high-field states $|T_+\rangle$, $|T_0\rangle$, $|T_-\rangle$.^[30, 31] The splitting of the triplet sublevels thereby depends on the orientation of the external magnetic field \vec{B} with respect to the principal axes X, Y, and Z of the ZFS tensor.^[30] The energy of the aligned state, called canonical orientation, is thus independent of B and equal to the energy at zero field, while the energies of the other two states increase/decrease with magnetic field (Figure S11).^[31] The population of the high-field state is therefore different for each canonical orientation:^[30, 31]

$$\vec{B}||Z: p_0 = p_z, p_{\pm} = 0.5 (p_x + p_y)$$

$$\vec{B}||Y: p_0 = p_y, p_{\pm} = 0.5 (p_x + p_z)$$

$$\vec{B}||X: p_0 = p_x, p_{\pm} = 0.5 (p_y + p_z)$$

For each orientation of the principal axis of \mathbf{D} with respect to \vec{B} , there are enhanced absorptive and emissive transitions in magnetic resonant conditions (Figure S11), which add up in rigid samples to a characteristic powder pattern.^[30]

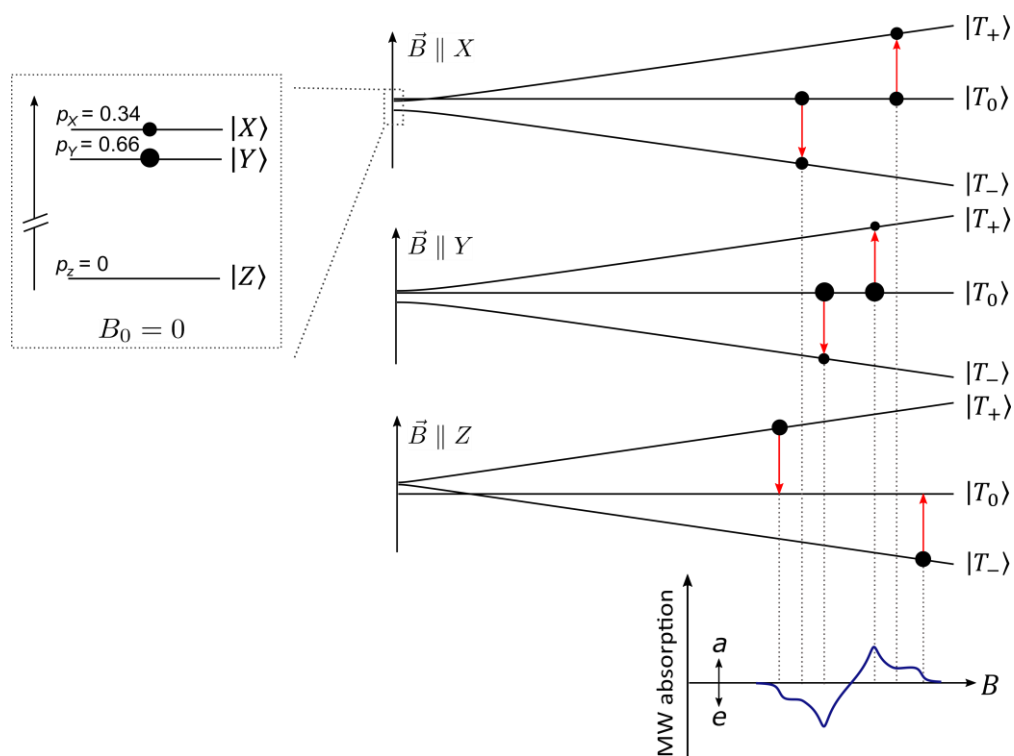


Figure S11. Generation of a Y6 trEPR spectrum with $[\rho_z, \rho_y, \rho_x] = [0, 0.66, 0.34]$. ISC is sublevel selective and acts on the zero-field sublevels $|X\rangle$, $|Y\rangle$ and $|Z\rangle$. These populations are converted into high-field populations $|T_+\rangle$, $|T_0\rangle$ and $|T_-\rangle$, depending on the principal axes (X, Y, Z) orientation of the ZFS tensor \mathbf{D} with respect to magnetic field \vec{B} . The aligned state is thereby energetically independent of the external magnetic field, while the other two states increase/decrease with B . The unequal populations result in microwave emission (e) or absorption (a) for $\Delta m_s = \pm 1$ transitions (purple) for each canonical orientation. The spectra of all orientations of \mathbf{D} relative to \vec{B} add up to a characteristic trEPR signal (blue). (adapted from Ref.^[30])

trEPR Pattern by Geminate Back Charge Transfer

Molecular triplet excitons occupied by geminate back charge transfer (BCT) can be distinguished from SOC-driven ISC by another pattern in the trEPR signal. The spin-polarization on the triplet sublevels is thereby converted from the CT states. As already explained in the main text, CT states can be explained in the context of a spin-correlated radical pair (SCRPs) whereby spin mixing occurs only between states $|^3\text{CT}_0\rangle$ and $|^1\text{CT}_0\rangle$ ($m_s = 0$). Thus, regarding the triplet sublevels, only $|^3\text{CT}_0\rangle$ is occupied. If charge transfer excitons undergo spin-allowed BCT to triplet excitons with shorter spin-spin distances, i.e. molecular triplet states, the spin polarization is preserved. The overpopulated $|T_0\rangle$ state thus leads to an *aeaeae* or *eaeeea* pattern as shown in Figure S12. This pattern can only be obtained by selective population of high-field spin states and can thus be distinguished from triplet excitons occupied by SOC-driven ISC.

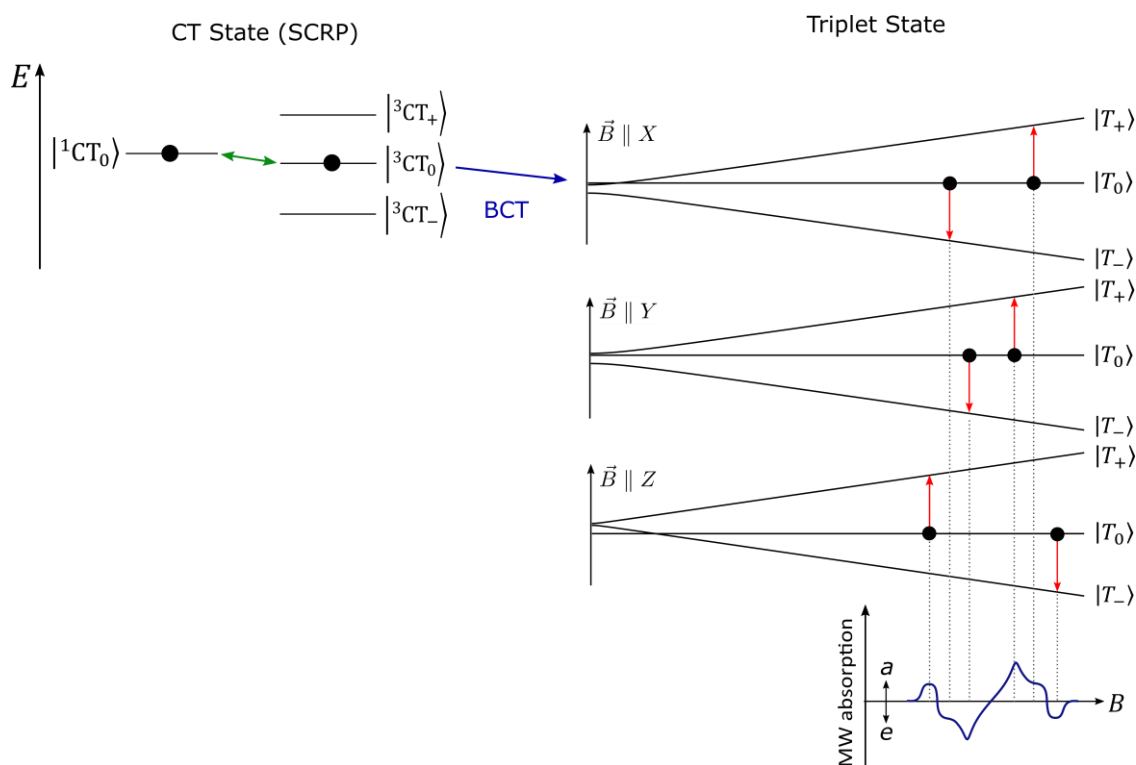


Figure S12. Generation of a trEPR spectrum generated by geminate BCT. Due to angular momentum conservation, spin mixing occurs only between $|^3CT_0\rangle$ and $|^1CT_0\rangle$ ($m_s = 0$). Spin-allowed BCT to triplet excitons preserves spin polarization, whereby high-field $|T_0\rangle$ states get overpopulated, arising here in an *aeaae* pattern.

Additional trEPR Spectra

The following part shows trEPR spectra of polymers (Figure S13) and Y7 including blends (Figure S14).

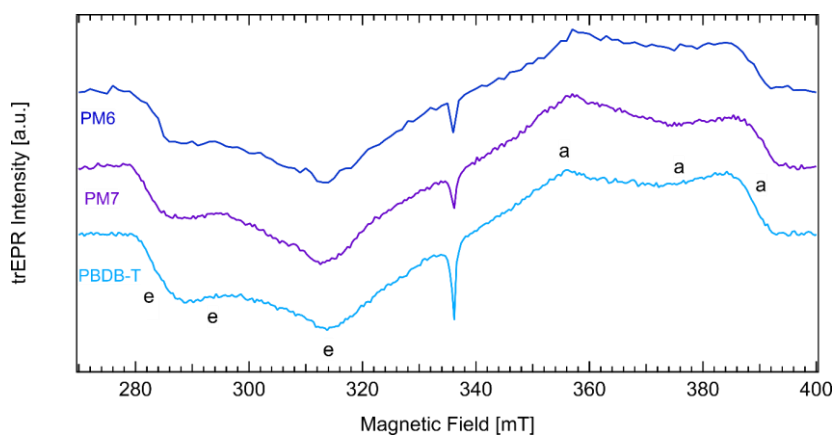


Figure S13. trEPR of neat PM6, PM7 and PBDB-T. All spectra show SOC-driven ISC pattern (*eeaae*) and a small CT contribution at 336.1 mT. Simulations including parameters are given below.

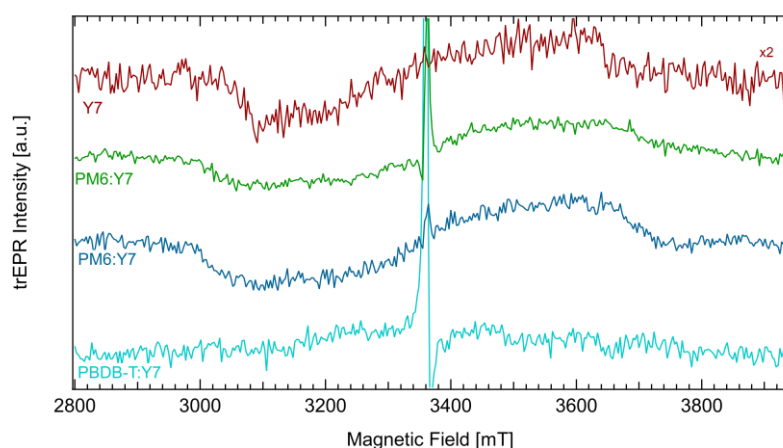


Figure S14. trEPR of neat Y7 and the blends PM6:Y7, PM7:Y7 and PBDB-T:Y7. All triplet spectra show a SOC-driven ISC pattern (*eeaaaa*). PBDB-T:Y7 shows negligible triplet yield by ISC, which is comparable to PBDB-T:Y6.

7. HOMO/LUMO Level

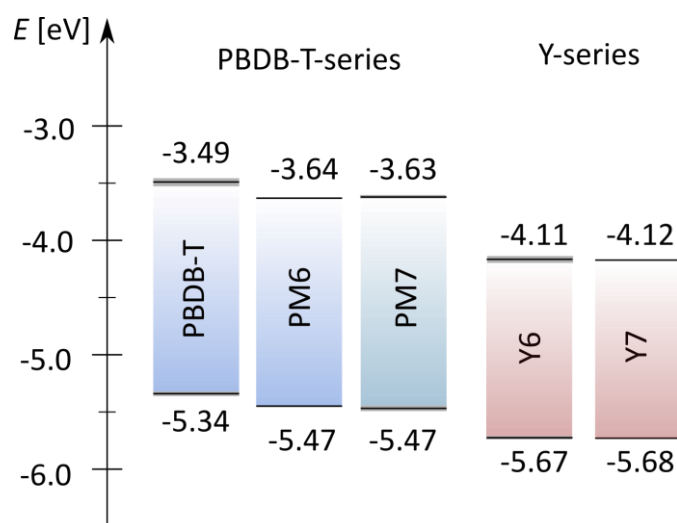


Figure S15. HOMO and LUMO levels of donors PBDB-T, PM6 and PM7 as well as acceptors Y6 and Y7. The HOMO of halogenated donors PM6 and PM7 are downshifted in comparison to non-halogenated PBDB-T. Thus, the HOMO offset and therefore the driving force for hole transfer of halogenated OPV blends PM6:Y6, PM7:Y6, PM7:Y6 and PM7:Y7 is lower than for PBDB-T:Y6 and PBDB-T:Y7. The values are given with the mean value and standard error taken from literature for PBDB-T^[32-35], PM6^[32, 34-37], PM7^[36-39], Y6^[13, 40-43], Y7^[44, 45].

8. Triplet Simulation Parameters

PLDMR

| Material | Triplet | | | | | CT | |
|-----------|----------------|------------------|------------------------------------|-------------------------|----------------------|--------------------|----------------|
| | D/h [MHz] | E/h [MHz] | $\lambda_\theta, \lambda_\phi$ | Lw [mT] | weight | Lw [mT] | weight |
| Y6 | 940 | 200* | 3.8 | [6.8 0] | 0.70 | [0 2.5] [0 0.9] | 0.30 - 0.19 |
| PBDB-T | 1500 | 120 120 | 7.1, 0 -1.5, 4.0 | [4.5 0] [0 8.9] | 0.37 0.27 | [1 1.4] | 0.36 |
| PM6 | 1510 | 120 120 75 | 11.4, 0 -2.0, 8.0 -1.0, -5.0 | [4 0] [0 8] [0 5] | 0.40 0.12 0.28 | [0 1] | 0.20 |
| PM7 | 1510 | 120 120 50 | 8.0, 0 -2.0, 7.0 -2.0, 0 | [4 0] [0 8] [0 7] | 0.48 0.20 0.20 | [0 1.4] | 0.12 |
| PBDB-T:Y6 | 1040 | 200* | 4.2, 0 | [7 0] | 0.20 | [0.8 1.9] | 0.80 |
| PM6:Y6 | 1020 | 200* | 5.5, 0 | [7 0] | 0.15 | [0.8 2.2] | 0.85 |
| PM7:Y6 | 1000 | 200* | 5.5, 0 | [7 0] | 0.38 | [0.9 2.5] | 0.62 |

Table S5. Parameter for PLDMR spectral simulations using the MATLAB tool EasySpin for spin-coated substrates. *: E value cannot be determined due to high ordering.

| Material | Triplet | | | | | CT | |
|-----------|----------------|------------------|-------------------------------------|-----------------------------|----------------------|----------------------|---------------|
| | D/h [MHz] | E/h [MHz] | $\lambda_\theta, \lambda_\phi$ | Lw [mT] | weight | Lw [mT] | weight |
| Y6 | 830 | 150 | 2.0, -1.0 | [8 0] | 0.56 | [1.1 0.8] [0 0.8] | 0.44 -0.19 |
| Y7 | 1040 | 230 | 0.5, -0.7 | [0 1.5] | 0.97 | [0 1.2] [0 0.83] | 0.03 -0.02 |
| PBDB-T | 1500 | 185 185 70 | 9.0, 0.0 -0.4, 2.8 -2.2, -1.0 | [3.5 0] [3.5 0] [3 0] | 0.13 0.3 0.07 | [0 1.5] | 0.51 |
| PM6 | 1510 | 170 170 75 | 8.0, 0.0 0.0, 3.5 -1.0, -2.5 | [4 0] [0 3.5] [0 3.5] | 0.1 0.66 0.02 | [0.3 0.9] | 0.22 |
| PM7 | 1530 | 200 200 80 | 9.0, 2.0 -0.6, 2.3 -4.5, -1.7 | [4 0] [4 0] [3.5 0] | 0.14 0.42 0.08 | [0 1.5] | 0.36 |
| PBDB-T:Y6 | 920 | 230 | 0.6, 2.2 | [10 0] | 0.03 | [1.2 0.9] | 0.97 |
| PM6:Y6 | 850 | 240 | 0.6, 0.2 | [5 0] | 0.04 | [0.8 1.1] | 0.96 |
| PM7:Y6 | 900 | 220 | 1.6, 2.0 | [15 0] | 0.16 | [0.6 1.9] | 0.84 |
| PBDB-T:Y7 | 1060 | 205 | 0.6, 0.6 | [9 0] | 0.06 | [0.5 1.5] | 0.94 |
| PM6:Y7 | 1100 | 240 | 1.2, 1.3 | [9 0] | 0.26 | [0.7 1.8] | 0.74 |
| PM7:Y7 | 1190 | 240 | -1.0, -3.0 | [9.5 0] | 0.26 | [1.0 2.0] | 0.74 |

Table S6. Parameter for PLDMR spectral simulations using the MATLAB tool EasySpin for dropcast samples.

Table S5 and S6 lists the EasySpin simulation parameters for PLDMR spectra of triplet excitons and CT states in the various pristine materials and blends. Parameters given are the ZFS parameters D and E ,

ordering factors λ_θ , λ_ϕ , the spectral linewidth with Gaussian and Lorentzian contributions [Gaussian Lorentzian] and the weight of the signals (relative signal intensity). The ordering factor λ specifies the orientational distribution of the molecules in the sample and is reflected by “wings” in the PLDMR spectrum.^[46, 47] The ordering is more pronounced in PLDMR than in trEPR, as seen in previous studies.^[48] The ordering factor λ is given for θ and ϕ , whereby θ is the angle between the molecular z-axis and static magnetic field B_0 and ϕ is the in-plane angle. If the ordering factor λ is zero, all molecular orientations occur with the same probability. The weight is the relative intensity of the spectral contributions of superimposed triplet and CT spectra.

The polymers PBDB-T, PM6 and PM7 show triplet excitons with different ordering: All triplet excitons possess the same dipolar interaction (D value), whereby we found two different E values, i.e. value for the rhombicity or the non-axial symmetry, indicating different internal arrangement.^[49] These different triplet excitons have a preferred orientational distribution, given by the ordering factors. The NFAs possess a broader CT peak (comparable to blends) and a small negative CT contribution. All blends possess a high weight in the CT peak due to additional CT states. All the blends with NFA Y7 show triplet contribution on the NFA. The D value of Y7 and its blends is higher than NFA Y6 and its blends.

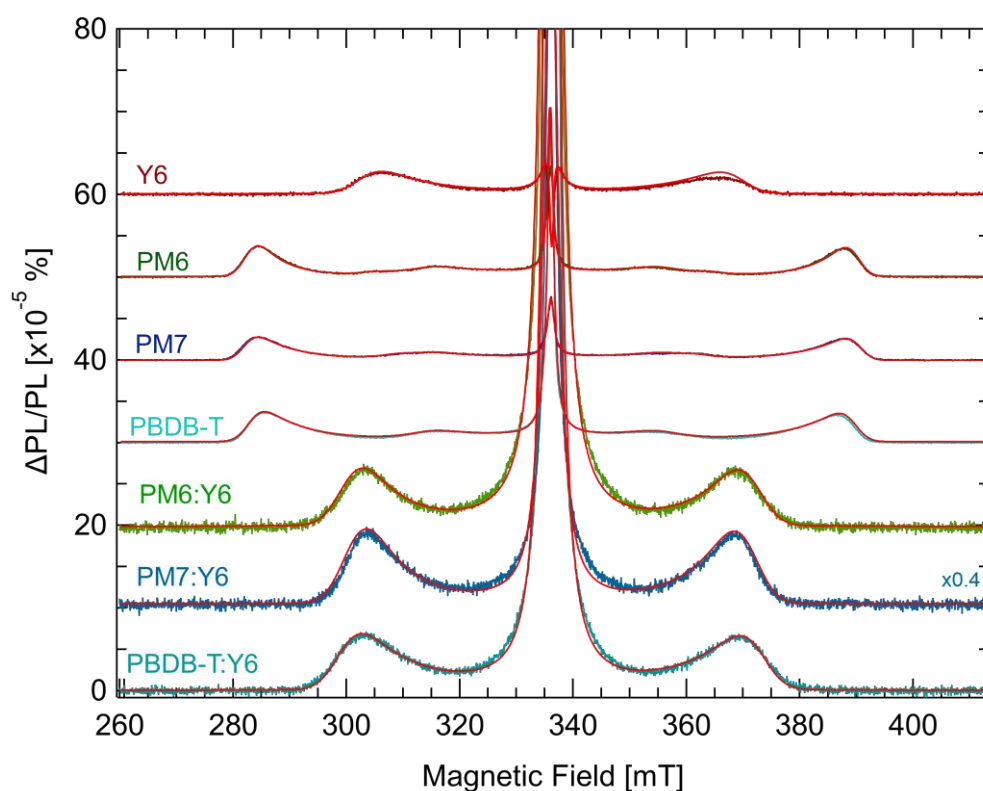


Figure S16. EasySpin Simulations (red) of all PLDMR measurements on spin-coated substrates (colored).

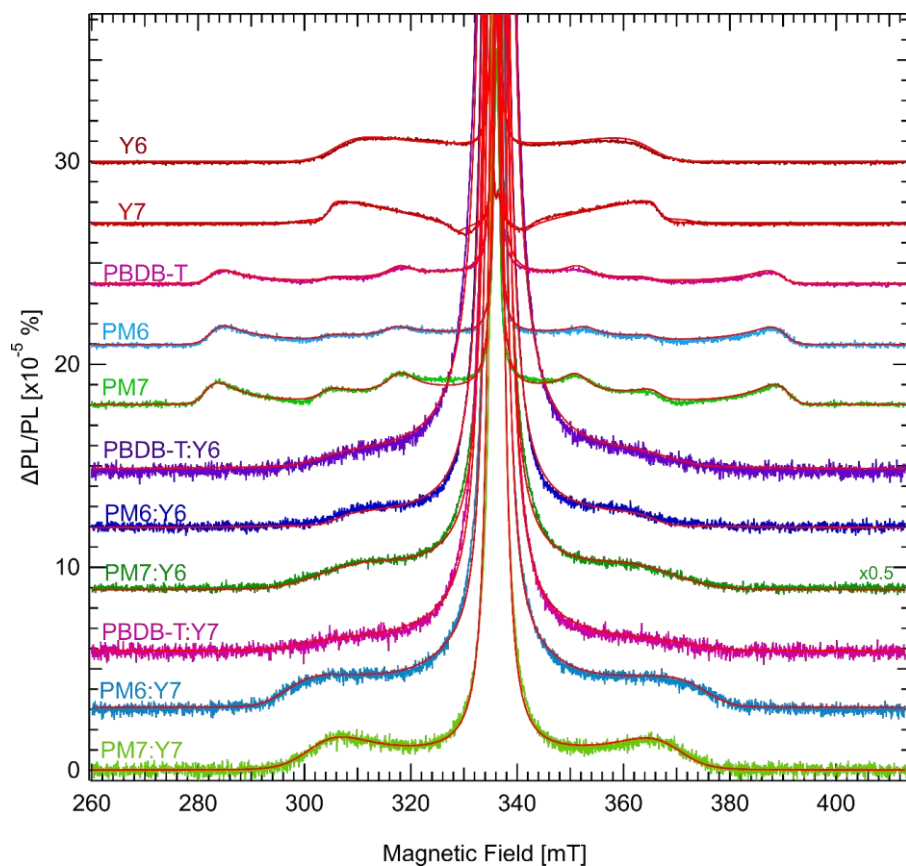


Figure S17. EasySpin Simulations (red) of all PLDMR measurements (colored).

trEPR

| Material | D/h [MHz] | E/h [MHz] | $[p_z, p_y, p_x]$ | $\lambda_\theta, \lambda_\phi$ | Lw [mT] |
|----------|-------------|-------------|-------------------|--------------------------------|---------|
| Y6 | 945 | 215 | [0.00 0.66 0.34] | 0, 0 | [0 2] |
| Y7 | 850 | 240 | [0.00 0.62 0.42] | 0, 0 | [0 1.5] |
| PBDB-T | 1460 | 95 | [0.00 0.51 0.49] | 0.68, 0.44 | [0 2.3] |
| PM6 | 1455 | 100 | [0.00 0.56 0.44] | 0.42, -0.1 | [0 2.7] |
| PM7 | 1510 | 120 | [0.00 0.53 0.47] | 0.35, 0.1 | [0 2.0] |
| PM6:Y6 | 995 | 210 | [0.00 0.66 0.34] | 0.42, -0.1 | [0 3.2] |
| PM7:Y6 | 880 | 160 | [0.00 0.66 0.34] | 0.35, 0.1 | [0 2.0] |
| PM6:Y7 | 900 | 200 | [0 0.60 0.40] | 0.42, -0.1 | [0 4] |
| PM7:Y7 | 925 | 200 | [0 0.60 0.40] | 0.35, -1.0 | [0 2.1] |

Table S7. Parameter for trEPR spectral simulations using the MATLAB tool EasySpin.

Table S7 lists the EasySpin simulation parameters for trEPR spectra of triplet excitons in the various pristine materials and blends. Parameters given are the ZFS parameters D and E , relative zero-field populations, ordering factors $\lambda_\theta, \lambda_\phi$ and the spectral linewidth with Gaussian and Lorentzian contributions [Gaussian Lorentzian].

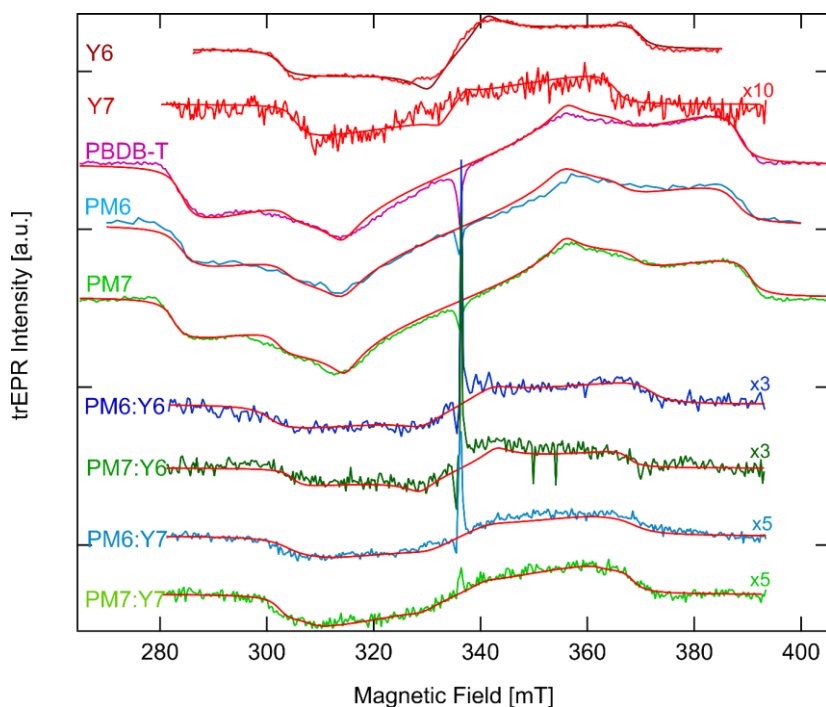


Figure S18. EasySpin Simulations (red) of trEPR measurements (colored).

References

- [1] M. S. Kotova, G. Londi, J. Junker, S. Dietz, A. Privitera, K. Tvingstedt, D. Beljonne, A. Sperlich and V. Dyakonov, *Mater. Horiz.* **2020**, *7*, 1641-1649.
- [2] G. Han, T. Hu and Y. Yi, *Adv. Mater.* **2020**, *32*, 2000975.
- [3] L. Perdigón-Toro, H. Zhang, A. Markina, J. Yuan, S. M. Hosseini, C. M. Wolff, G. Zuo, M. Stolterfoht, Y. Zou and F. Gao, *Adv. Mater.* **2020**, *32*, 1906763.
- [4] K. Wang, H. Chen, J. Zhang, Y. Zou and Y. Yang, *J. Phys. Chem. Lett.* **2021**, *12*, 3928-3933.
- [5] K. Zhou, Y. Liu, A. Alotaibi, J. Yuan, C. Jiang, J. Xin, X. Liu, B. A. Collins, F. Zhang and W. Ma, *ACS Energy Lett.* **2020**, *5*, 589-596.
- [6] G. Li, X. Zhang, L. O. Jones, J. M. Alzola, S. Mukherjee, L.-w. Feng, W. Zhu, C. L. Stern, W. Huang and J. Yu, *J. Am. Chem. Soc.* **2021**, *143*, 6123-6139.
- [7] A. Karki, J. Vollbrecht, A. L. Dixon, N. Schopp, M. Schrock, G. M. Reddy and T. Q. Nguyen, *Adv. Mater.* **2019**, *31*, 1903868.
- [8] L. Perdigón-Toro, L. Q. Phuong, S. Zeiske, K. Vandewal, A. Armin, S. Shoaee and D. Neher, *ACS Energy Lett.* **2021**, *6*, 557-564.
- [9] R. Wang, C. Zhang, Q. Li, Z. Zhang, X. Wang and M. Xiao, *J. Am. Chem. Soc.* **2020**, *142*, 12751-12759.
- [10] S. Li, C.-Z. Li, M. Shi and H. Chen, *ACS Energy Lett.* **2020**, *5*, 1554-1567.
- [11] Y. Cui, H. Yao, J. Zhang, T. Zhang, Y. Wang, L. Hong, K. Xian, B. Xu, S. Zhang and J. Peng, *Nat. Commun.* **2019**, *10*, 1-8.
- [12] L. Qin, X. Liu, X. Zhang, J. Yu, L. Yang, F. Zhao, M. Huang, K. Wang, X. Wu and Y. Li, *Angew. Chem. Int. Ed.* **2020**, *59*, 15043-15049.
- [13] M. Zhang, L. Zhu, G. Zhou, T. Hao, C. Qiu, Z. Zhao, Q. Hu, B. W. Larson, H. Zhu and Z. Ma, *Nat. Commun.* **2021**, *12*, 1-10.
- [14] A. J. Gillett, A. Privitera, R. Dilmurat, A. Karki, D. Qian, A. Pershin, G. Londi, W. K. Myers, J. Lee, J. Yuan, S.-J. Ko, M. Riede, F. Gao, G. Bazan, A. Rao, T.-Q. Nguyen, D. Beljonne and R. H. Friend, *Nature* **2021**, *597*, 5.

- [15] L. Ma, H. Yao, J. Wang, Y. Xu, M. Gao, Y. Zu, Y. Cui, S. Zhang, L. Ye and J. Hou, *Angew. Chem.* **2021**.
- [16] R. Ma, G. Li, D. Li, T. Liu, Z. Luo, G. Zhang, M. Zhang, Z. Wang, S. Luo and T. Yang, *Solar RRL* **2020**, 4, 2000250.
- [17] F. D. Eisner, M. Azzouzi, Z. Fei, X. Hou, T. D. Anthopoulos, T. J. S. Dennis, M. Heeney and J. Nelson, *Journal of the American Chemical Society* **2019**, 141, 6362-6374.
- [18] L. Zhu, M. Zhang, G. Zhou, T. Hao, J. Xu, J. Wang, C. Qiu, N. Prine, J. Ali and W. Feng, *Adv. Energy Mater.* **2020**, 10, 1904234.
- [19] R. Ma, T. Yang, Y. Xiao, T. Liu, G. Zhang, Z. Luo, G. Li, X. Lu, H. Yan and B. Tang, *Energy Environ. Mater.* **2021**.
- [20] P. S. Marqués, G. Londi, B. Yurash, T.-Q. Nguyen, S. Barlow, S. R. Marder and D. Beljonne, *Chemical science* **2021**, 12, 7012-7022.
- [21] S. Hirata and M. Head-Gordon, *Chem. Phys. Lett.* **1999**, 314, 291-299.
- [22] S. Refaely-Abramson, S. Sharifzadeh, N. Govind, J. Autschbach, J. B. Neaton, R. Baer and L. Kronik, *Phys. Rev. Lett.* **2012**, 109, 226405.
- [23] T. Stein, H. Eisenberg, L. Kronik and R. Baer, *Phys. Rev. Lett.* **2010**, 105, 266802.
- [24] M. J. Frisch, G. W. Trucks, H. B. Schlegel, G. E. Scuseria, M. A. Robb, J. R. Cheeseman, G. Scalmani, V. Barone, G. A. Petersson, H. Nakatsuji, X. Li, M. Caricato, A. V. Marenich, J. Bloino, B. G. Janesko, R. Gomperts, B. Mennucci, H. P. Hratchian, J. V. Ortiz, A. F. Izmaylov, J. L. Sonnenberg, Williams, F. Ding, F. Lipparini, F. Egidi, J. Goings, B. Peng, A. Petrone, T. Henderson, D. Ranasinghe, V. G. Zakrzewski, J. Gao, N. Rega, G. Zheng, W. Liang, M. Hada, M. Ehara, K. Toyota, R. Fukuda, J. Hasegawa, M. Ishida, T. Nakajima, Y. Honda, O. Kitao, H. Nakai, T. Vreven, K. Throssell, J. A. Montgomery Jr., J. E. Peralta, F. Ogliaro, M. J. Bearpark, J. J. Heyd, E. N. Brothers, K. N. Kudin, V. N. Staroverov, T. A. Keith, R. Kobayashi, J. Normand, K. Raghavachari, A. P. Rendell, J. C. Burant, S. S. Iyengar, J. Tomasi, M. Cossi, J. M. Millam, M. Klene, C. Adamo, R. Cammi, J. W. Ochterski, R. L. Martin, K. Morokuma, O. Farkas, J. B. Foresman and D. J. Fox, Gaussian, Inc., Wallingford CT, 2016.
- [25] X. Gao, S. Bai, D. Fazzi, T. Niehaus, M. Barbatti and W. Thiel, *J. Chem. Theory Comput.* **2017**, 13, 515-524.
- [26] Y. Li, H. Meng, J. Huang and C. Zhan, *ACS Appl. Mater. Interfaces* **2020**, 12, 50541-50549.
- [27] G. Zhang, X.-K. Chen, J. Xiao, P. C. Chow, M. Ren, G. Kupgan, X. Jiao, C. Chan, X. Du and R. Xia, *Nat. Commun.* **2020**, 11, 1-10.
- [28] J. Yuan, Y. Zhang, L. Zhou, G. Zhang, H.-L. Yip, T.-K. Lau, X. Lu, C. Zhu, H. Peng and P. A. Johnson, *Joule* **2019**, 3, 1140-1151.
- [29] E. Hontz, W. Chang, D. N. Congreve, V. Bulović, M. A. Baldo and T. Van Voorhis, *J. Phys. Chem. C* **2015**, 119, 25591-25597.
- [30] S. Weber, *eMagRes* **2007**, 255-270.
- [31] S. Richert, C. E. Tait and C. R. Timmel, *J. Magn. Reson.* **2017**, 280, 103-116.
- [32] X. Li, R. Ma, T. Liu, Y. Xiao, G. Chai, X. Lu, H. Yan and Y. Li, *Science China Chemistry* **2020**, 63, 1256-1261.
- [33] Y. Bai, B. Yang, X. Chen, F. Wang, T. Hayat, A. Alsaedi and Z. a. Tan, *Front. Chem.* **2018**, 6, 292.
- [34] Y.-J. Xue, F.-Y. Cao, P.-K. Huang, Y.-C. Su and Y.-J. Cheng, *J. Mater. Chem. A* **2020**, 8, 5315-5322.
- [35] Y. Zhang, H. Feng, L. Meng, Y. Wang, M. Chang, S. Li, Z. Guo, C. Li, N. Zheng and Z. Xie, *Adv. Energy Mater.* **2019**, 9, 1902688.
- [36] R. Ma, T. Liu, Z. Luo, Q. Guo, Y. Xiao, Y. Chen, X. Li, S. Luo, X. Lu and M. Zhang, *Sci. China: Chem* **2020**, 63, 325-330.
- [37] J. Zhang, Y. Han, W. Zhang, J. Ge, L. Xie, Z. Xia, W. Song, D. Yang, X. Zhang and Z. Ge, *ACS Appl. Mater. Interfaces* **2020**, 12, 57271-57280.
- [38] C. K. Wang, B. H. Jiang, J. H. Lu, M. T. Cheng, R. J. Jeng, Y. W. Lu, C. P. Chen and K. T. Wong, *ChemSusChem* **2020**, 13, 903-913.
- [39] J. Fang, Q. Liu, J. Zhang, L. Ye, J. Wu, Z. Wei, X. Guo, M. Zhang and Y. Li, *Solar RRL* **2020**, 4, 2000275.

- [40] T. Liu, R. Ma, Z. Luo, Y. Guo, G. Zhang, Y. Xiao, T. Yang, Y. Chen, G. Li and Y. Yi, *Energy Environ. Sci.* **2020**, *13*, 2115-2123.
- [41] W. Tang, W. Peng, M. Zhu, H. Jiang, W. Wang, H. Xia, R. Yang, O. Inganäs, H. Tan and Q. Bian, *J. Mater. Chem. A* **2021**, *9*, 20493-20501.
- [42] Y. Chen, T. Liu, L.-K. Ma, W. Xue, R. Ma, J. Zhang, C. Ma, H. K. Kim, H. Yu and F. Bai, *J. Mater. Chem. A* **2021**, *9*, 7481-7490.
- [43] X. Xu, K. Feng, Z. Bi, W. Ma, G. Zhang and Q. Peng, *Adv. Mater.* **2019**, *31*, 1901872.
- [44] H.-C. Wang, C.-H. Chen, R.-H. Li, Y.-C. Lin, C.-S. Tsao, B. Chang, S. Tan, Y. Yang and K.-H. Wei, *Solar RRL* **2020**, *4*, 2000253.
- [45] T. Gokulnath, J. Choi, H.-Y. Park, K. Sung, Y. Do, H. Park, J. Kim, S. S. Reddy, J. Kim and M. Song, *Nano Energy* **2021**, *89*, 106323.
- [46] T. Biskup, M. Sommer, S. Rein, D. L. Meyer, M. Kohlstädt, U. Würfel and S. Weber, *Angew. Chem. Int. Ed.* **2015**, *54*, 7707-7710.
- [47] <https://easyspin.org/easyspin/documentation/pepper.html>
- [48] A. Privitera, J. Grüne, A. Karki, W. K. Myers, V. Dyakonov, T. Q. Nguyen, M. K. Riede, R. H. Friend, A. Sperllich and A. J. Gillett, *Adv. Energy Mater.* **2022**, 2103944.
- [49] J. Telsler, *EPR Spectroscopy: Fundamentals and Methods* **2018**, 29.